No. 574 **July 2017**

An entropy stable spacetime discontinuous Galerkin method for the two-dimensional compressible Navier-Stokes equations

A. Hiltebrand, S. May

ISSN: 2190-1767

An entropy stable spacetime discontinuous Galerkin method for the two-dimensional compressible Navier-Stokes equations*

Andreas Hiltebrand† and Sandra May ‡

In this paper, we present an entropy stable scheme for solving the compressible Navier-Stokes equations in two space dimensions. Our scheme uses entropy variables as degrees of freedom. It is an extension of an existing spacetime discontinuous Galerkin method for solving the compressible Euler equations. The physical diffusion terms are incorporated by means of the symmetric (SIPG) or nonsymmetric (NIPG) interior penalty method, resulting in the two versions ST-SDSC-SIPG and ST-SDSC-NIPG. The streamline diffusion and shock-capturing terms from the original scheme have been kept, but have been adjusted appropriately. This guarantees that the new scheme essentially reduces to the original scheme for the compressible Euler equations in regions with underresolved physical diffusion. We show entropy stability for both versions under suitable assumptions. We also present numerical results confirming the accuracy and robustness of our schemes.

Keywords. Discontinuous Galerkin method, compressible Navier-Stokes equations, entropy stability, entropy variables, interior penalty method, wall boundary conditions.

1. Introduction

In this contribution, we present schemes for solving the compressible Navier-Stokes equations in two space dimensions that are proven to be entropy stable. Our schemes are extensions of the method by Hiltebrand and Mishra [20, 19] for solving hyperbolic systems of conservation laws. We use a version specific to the compressible Euler equations. The scheme by Hiltebrand and Mishra has the following features: it uses entropy variables as degrees of freedom (instead of the classic conserved variables), uses a spacetime (ST) discontinuous Galerkin (DG) approach on unstructured grids, and involves streamline diffusion (SD) and shock-capturing (SC) terms. As a result, the scheme can be shown to be entropy stable, is unconditionally stable, is (arbitrarily) high-order in smooth flow, and is robust in the presence of shocks and discontinuities.

We extend the scheme to solving the compressible Navier-Stokes equations by adding a suitable treatment for the physical diffusion terms representing viscosity and heat conduction.

*This work was supported by ERC STG. N 306279, SPARCCLE

†Formerly: Seminar for Applied Mathematics, ETH Zurich, Rämistrasse 101, 8092 Zurich, Switzerland

‡TU Dortmund, Vogelpothsweg 87, 44227 Dortmund, Germany, sandra.may@math.tu-dortmund.de

We consider both the nonsymmetric (NIPG) and symmetric (SIPG) interior penalty formulation for this purpose, resulting in the versions ST-SDSC-NIPG and ST-SDSC-SIPG. In our extension, we preserve all the positive qualities of the original scheme. In particular, we can show entropy stability of the resulting numerical scheme under suitable conditions for both ST-SDSC-NIPG and ST-SDSC-SIPG.

The question of whether one still needs streamline diffusion and shock-capturing terms when approximating the compressible Navier-Stokes equations is quite controversial. For efficiency reasons, the physical diffusion cannot be resolved everywhere in a typical computation. In regions where the physical diffusion is sufficiently resolved, e.g., in boundary layers, the additional diffusion terms are not needed. Away from boundaries, the solution of the compressible Navier-Stokes equations can behave quite similar to the solution of the compressible Euler equations when the physical diffusion is not sufficiently resolved. In these regions, we want to ensure that our scheme essentially reduces to the original scheme by Hiltebrand and Mishra. Therefore, we do include a suitable extension of the original SD and SC terms in our new schemes. The artificial diffusion terms are constructed such that they eliminate most oscillations around shocks and vanish with the correct order of convergence in smooth flow. In particular we observe for smooth flow convergence orders of $O(h^{k+1})$ for polynomial degrees of order k (with a potentially worse rate for the ST-SDSC-NIPG version for even polynomial degree k).

In the literature, there exists a variety of DG methods for solving the compressible Navier-Stokes equations that are based on discretizing the *conserved* variables of the system, see, e.g., [4, 5, 6, 7, 8, 9, 10, 11, 12, 13, 15, 17, 18, 30] and the references cited therein. Several of them use the IP method for discretizing the diffusion term for example the work by Hartmann and Houston [17, 18]. Others use, e.g., the local discontinuous Galerkin (LDG) approach or the 'Bassi-Rebay' approach. A unified comparison of typical discretizations for the diffusion terms can be found in [1] for the case of an elliptic model problem. To the best of our knowledge the above methods do not allow for theoretical stability results for the case of the actual diffusion operator of the compressible Navier-Stokes equations.

Though to a smaller extent, there is also some work based on using *entropy* variables as degrees of freedom. In [21], Hughes et al. examine the properties of the physical diffusion and heat conduction terms for the compressible Navier-Stokes equations when entropy variables are used as degrees of freedom. In [34], Shakib et al. use a spacetime finite element approach for solving the resulting equations. The authors use discontinuous elements in time but continuous elements in space. Barth [2, 3] uses a spacetime DG approach and discretizes the diffusion term using the SIPG approach. To the best of our knowledge though he does not examine entropy stability for the actual discrete formulation nor does he include shock-capturing terms for simulations for the Navier-Stokes equations. Further, van der Vegt and coworkers [27, 26, 32] have worked on solving the compressible Navier-Stokes equations using both conserved variables and entropy variables. The authors use a spacetime DG approach in combination with an IP discretization of the diffusion term but also do not provide an explicit proof of entropy stability. The work by Zakerzadeh and G. May [39] is one of the few ones that does provide entropy stability estimates for the fully discrete versions. The authors examine entropy stability for different discretizations of the diffusion term, in particular for a LDG discretization, a BR2-type discretization, and also a form of the SIPG discretization. However, the specific version of the employed SIPG discretization is different from the one considered here. Further, the authors do not include shock-capturing terms and do not consider boundary contributions. Finally, May [29, 28] compares one-dimensional extensions of the scheme by Hiltebrand and

Mishra using the IP discretization and the LDG discretization for the diffusion term and provides corresponding entropy stability results.

In this contribution, we extend the method based on IP discretization to two dimensions. The proof of entropy stability for the SIPG approach is more challenging in two dimensions as the 8×8 diffusion matrix written with respect to entropy variables only has rank 5. We also examine the case of adiabatic solid wall boundary conditions here whereas all of the above mentioned contributions assume compact support of the solution. Furthermore, we provide improved artificial diffusion terms compared to [29] as well as extensive numerical results in two dimensions.

This paper is structured as follow: in section 2, we shortly review the original scheme of Hiltebrand and Mishra for solving hyperbolic systems of conservation laws to keep this work self-contained. In section 3, we discuss properties of the compressible Navier-Stokes equations in two dimensions when entropy variables are used as degrees of freedom. In section 4, we present our extensions ST-SDSC-SIPG and ST-SDSC-NIPG for solving the compressible Navier-Stokes equations. This includes the discretization of the physical diffusion term as well as the suitable extension of the artificial diffusion terms. In section 5, we show entropy stability of our schemes under suitable assumptions. Finally, in section 6 we present numerical results in one and two space dimensions for piecewise polynomial spaces of degrees one, two, and three. We conclude with a summary in section 7.

2. Review of the spacetime DG method for hyperbolic systems

In this section, we review the spacetime DG formulation for systems of hyperbolic conservation laws that our new method is based on to keep this work self-contained. For more detailed information, we refer to [20, 19].

Consider a system of hyperbolic conservation laws on the open domain $\Omega \subset \mathbb{R}^2$ given by

$$\mathbf{U}_t + \mathbf{F}^1(\mathbf{U})_{x_1} + \mathbf{F}^2(\mathbf{U})_{x_2} = 0, \quad (\mathbf{x}, t) \in \Omega \times \mathbb{R}_+, \tag{1}$$

where $\mathbf{U} = (u_1, \dots, u_m)^T : \Omega \times \mathbb{R}_+ \to \mathbb{R}^m, m \in \mathbb{N}$, is the vector of conserved variables and $\mathbf{F}^k : \mathbb{R}^m \to \mathbb{R}^m$ is the flux function in x_k-direction, $k = 1, 2$. We use the short-hand notation $\mathbf{U}_t = \partial_t \mathbf{U}$ and $\mathbf{F}(\mathbf{U})_{x_k} = \partial_{x_k} \mathbf{F}(\mathbf{U})$. We assume the existence of a strictly convex entropy function $S : \mathbb{R}^m \to \mathbb{R}$ and of entropy flux functions $Q^k : \mathbb{R}^m \to \mathbb{R}$, $k = 1, 2$, such that the corresponding entropy inequality is satisfied. We note that this assumption is satisfied for the compressible Euler equations. One can then define *entropy variables* $\mathbf{V} = S_{\mathbf{U}}(\mathbf{U}) := \left(\frac{\partial S(\mathbf{U})}{\partial u_1}, \dots, \frac{\partial S(\mathbf{U})}{\partial u_m}\right)^T$ and apply a change of variables to get

$$\mathbf{U}(\mathbf{V})_t + \mathbf{F}^1(\mathbf{V})_{x_1} + \mathbf{F}^2(\mathbf{V})_{x_2} = 0, \quad (\mathbf{x}, t) \in \Omega \times \mathbb{R}_+, \tag{2}$$

where $\mathbf{F}^k(\mathbf{V}) = \mathbf{F}^k(\mathbf{U}(\mathbf{V}))$ for brevity. The method is based on using these entropy variables as degrees of freedom instead of the usual conserved variables. Before describing the discretization of equation (2), we will first set the prerequisites for the spacetime mesh.

At the n^{th} time level t^n, we denote the time step as $\Delta t^n = t^{n+1} - t^n$ and the update time interval as $I^n = (t^n, t^{n+1})$. For simplicity, we assume that the spatial domain $\Omega \subset \mathbb{R}^2$ is bounded and polyhedral and divided into a triangulation $\mathcal{T}$, i.e., a non-overlapping set of triangles K such that $\cup_{K \in \mathcal{T}} \bar{K} = \bar{\Omega}$. Furthermore, we take the usual conditions of mesh and

shape regularity for granted. For a generic element (cell) K, we denote

$$\begin{aligned} h_K &= \operatorname{diam}(K), && \text{(diameter of } K\text{)}, \\ \mathcal{N}(K) &= \{K' \in \mathcal{T} : K' \neq K \wedge \operatorname{meas}_{1d}(\bar{K} \cap \bar{K}') > 0\}, && \text{(neighbours of } K\text{)}. \end{aligned}$$

The *mesh width* of the triangulation is $h(\mathcal{T}) = \max_K h_K$. A generic spacetime element is the prism $K \times I^n$. We also assume that there exists an (arbitrarily large) constant C such that $(1/C)h \leq \Delta t^n \leq Ch$ for all time levels n.

On a given triangulation $\mathcal{T}$ with mesh width $h(\mathcal{T})$, the discrete solution $\mathbf{V}^h$ (we will use the superscript h for referring to discrete variables) is sought in the space

$$\mathcal{V}^k = \left\{ \mathbf{W}^h \in \left(L^1(\Omega \times [0,T])\right)^m : \begin{array}{l} W_i^h|_{K\times I^n} \in \mathcal{P}^k(K \times I^n) \text{ in} \\ \text{each component } 1 \leq i \leq m \end{array} \right\}, \tag{3}$$

where $\mathcal{P}^k(K \times I^n)$ is the space of three-dimensional polynomials of order k on the prism $K \times I^n$. The discretization of the conservation law (2) is given by: find $\mathbf{V}^h \in \mathcal{V}^k$ such that

$$\mathcal{B}_{\mathrm{DG}}(\mathbf{V}^h, \mathbf{\Phi}^h) + \mathcal{B}_{\mathrm{SD}}(\mathbf{V}^h, \mathbf{\Phi}^h) + \mathcal{B}_{\mathrm{SC}}(\mathbf{V}^h, \mathbf{\Phi}^h) = 0 \quad \forall\, \mathbf{\Phi}^h \in \mathcal{V}^k. \tag{4}$$

In the following, we will give the details for each of the three quasilinear forms, which are all nonlinear in the first argument and linear in the second.

2.1. The DG quasilinear form

The form $\mathcal{B}_{\mathrm{DG}}$ is given by

$$\begin{aligned} \mathcal{B}_{\mathrm{DG}}(\mathbf{V}^h, \mathbf{\Phi}^h) = &- \sum_{n,K} \int_{I^n} \int_K \left(\mathbf{U}(\mathbf{V}^h) \cdot \mathbf{\Phi}_t^h + \sum_{k=1}^{2} \mathbf{F}^k(\mathbf{V}^h) \cdot \mathbf{\Phi}_{x_k}^h \right) d\mathbf{x}\, dt \\ &+ \sum_{n,K} \int_K \mathbb{U}(\mathbf{V}_{n+1,-}^h, \mathbf{V}_{n+1,+}^h) \cdot \mathbf{\Phi}_{n+1,-}^h d\mathbf{x} - \sum_{n,K} \int_K \mathbb{U}(\mathbf{V}_{n,-}^h, \mathbf{V}_{n,+}^h) \cdot \mathbf{\Phi}_{n,+}^h \, d\mathbf{x} \\ &+ \sum_{n,K} \sum_{K' \in \mathcal{N}(K)} \int_{I^n} \int_{\partial_{KK'}} \mathbb{F}(\mathbf{V}_{K,-}^h, \mathbf{V}_{K,+}^h; \nu_{KK'}) \cdot \mathbf{\Phi}_{K,-}^h \, d\sigma(\mathbf{x})\, dt, \end{aligned} \tag{5}$$

with

$$\begin{aligned} \mathbf{\Phi}_{n,\pm}^h(\mathbf{x}) &= \lim_{\varepsilon \to 0+} \mathbf{\Phi}^h(\mathbf{x}, t^n \pm \varepsilon) \\ \partial_{KK'} &= \bar{K} \cap \bar{K}', \\ \nu_{KK'} &= \text{unit normal for edge } KK' \text{ pointing outwards from element } K, \\ \mathbf{\Phi}_{K,\pm}^h(\mathbf{x}, t) &= \lim_{\varepsilon \to 0+} \mathbf{\Phi}^h(\mathbf{x} \pm \varepsilon \nu_{KK'}, t), \quad \forall \mathbf{x} \in \partial_{KK'}, \end{aligned} \tag{6}$$

for all $\mathbf{\Phi}^h \in \mathcal{V}^k$, and $\mathbf{a} \cdot \mathbf{b} = \sum_{i=1}^m a_i b_i$ for $\mathbf{a}, \mathbf{b} \in \mathbb{R}^m$.

We still need to specify the numerical fluxes that we use. To enable time marching, we choose the *upwind* flux for the temporal numerical flux $\mathbb{U}$:

$$\mathbb{U}(\mathbf{V}_{n,-}^h, \mathbf{V}_{n,+}^h) = \mathbf{U}(\mathbf{V}_{n,-}^h). \tag{7}$$

For the spatial numerical flux $\mathbb{F}$, we use a consistent, conservative, and *entropy-stable* flux given by

$$\mathbb{F}(\mathbf{V}^h_{K,-}, \mathbf{V}^h_{K,+}; \nu_{KK'}) = \sum_{k=1}^{2} \mathbb{F}^{k,*}(\mathbf{V}^h_{K,-}, \mathbf{V}^h_{K,+}) \nu^k_{KK'} - \frac{1}{2}\mathbb{D}(\mathbf{V}^h_{K,+} - \mathbf{V}^h_{K,-}) \tag{8}$$

with $\mathbb{D} = \mathbb{D}(\mathbf{V}^h_{K,-}, \mathbf{V}^h_{K,+}; \nu_{KK'})$. Here, $\mathbb{F}^{k,*}$ denotes an entropy-conservative flux (in x_k-direction). The existence of such fluxes for any generic conservation law with an entropy framework was shown by Tadmor [36]. Explicit expressions of entropy-conservative fluxes for the compressible Euler equations have been obtained, e.g., by Ismail and Roe [22]. The operator $\mathbb{D}$ represents a numerical diffusion operator. For detailed information – also concerning the entropy-conservative fluxes – we refer to [20, 19].

2.2. Streamline diffusion and shock-capturing operator

If one only used the $\mathcal{B}_{\mathrm{DG}}$-form, i.e., if one defined the discrete solution as the solution of $\mathcal{B}_{\mathrm{DG}}(\mathbf{V}^h, \mathbf{\Phi}^h) = 0 \; \forall \, \mathbf{\Phi}^h \in \mathcal{V}^k$, then this solution would typically exhibit unphysical oscillations near shocks and contact discontinuities. Therefore, a streamline diffusion and a shock-capturing operator are added, compare (4). These terms add artificial diffusion where needed in order to damp unphysical oscillations.

The following form is used for the streamline diffusion operator (cf. [20, 23, 25, 24])

$$\mathcal{B}_{\mathrm{SD}}(\mathbf{V}^h, \mathbf{\Phi}^h) = \sum_{n,K} \int_{I^n} \int_K \left(\mathbf{U}_{\mathbf{V}}(\mathbf{V}^h) \mathbf{\Phi}^h_t + \sum_{k=1}^{2} \mathbf{F}^k_{\mathbf{V}}(\mathbf{V}^h) \mathbf{\Phi}^h_{x_k} \right) \cdot \left(\mathbf{D}^{\mathrm{SD}}_{n,K} \mathrm{Res} \right) d\mathbf{x} \, dt \tag{9}$$

with intra-element residual

$$\mathrm{Res} = \mathbf{U}(\mathbf{V}^h)_t + \sum_{k=1}^{2} \mathbf{F}^k(\mathbf{V}^h)_{x_k}, \tag{10}$$

and scaling matrix

$$\mathbf{D}^{\mathrm{SD}}_{n,K} = C^{\mathrm{SD}} \Delta t^n \mathbf{U}^{-1}_{\mathbf{V}}(\mathbf{V}^h). \tag{11}$$

Here, C^{SD} denotes a positive constant and is typically chosen to be 10. Further, $\mathbf{U}_{\mathbf{V}}$ denotes the Jacobian $D\mathbf{U}(\mathbf{V})$ and $\mathbf{F}^k_{\mathbf{V}}$ the Jacobian $D\mathbf{F}^k(\mathbf{V})$. Note that the intra-element residual is well defined as the first derivatives are taken of a polynomial function.

The streamline diffusion operator adds numerical diffusion in the direction of the streamlines. However, one needs further numerical diffusion in order to reduce possible oscillations at shocks. For this purpose, the following shock-capturing operator (similar to Barth [2]) is used:

$$\mathcal{B}_{\mathrm{SC}}(\mathbf{V}^h, \mathbf{\Phi}^h) = \sum_{n,K} \int_{I^n} \int_K D^{\mathrm{SC}}_{n,K} \left(\mathbf{\Phi}^h_t \cdot \left(\widetilde{\mathbf{U}_{\mathbf{V}}} \mathbf{V}^h_t \right) + \sum_{k=1}^{2} \frac{{h_K}^2}{(\Delta t^n)^2} \mathbf{\Phi}^h_{x_k} \cdot \left(\widetilde{\mathbf{U}_{\mathbf{V}}} \mathbf{V}^h_{x_k} \right) \right) d\mathbf{x} \, dt, \tag{12a}$$

with $\widetilde{\mathbf{U}_{\mathbf{V}}} = \mathbf{U}_{\mathbf{V}}(\widetilde{\mathbf{V}}_{n,K})$ for brevity and

$$\widetilde{\mathbf{V}}_{n,K} = \frac{1}{\mathrm{meas}(I^n \times K)} \int_{I^n} \int_K \mathbf{V}^h(\mathbf{x}, t) \, d\mathbf{x} \, dt$$

being the cell average. The scaling factor is

$$D_{n,K}^{\mathrm{SC}} = \frac{\Delta t^n C^{\mathrm{SC}} \overline{\mathrm{Res}}_{n,K}}{\sqrt{\int_{I^n}\int_K \left(\mathbf{V}_t^h \cdot \left(\widetilde{\mathbf{U}_{\mathbf{V}}} \mathbf{V}_t^h \right) + \sum_{k=1}^{2} \frac{{h_K}^2}{(\Delta t^n)^2} \mathbf{V}_{x_k}^h \cdot \left(\widetilde{\mathbf{U}_{\mathbf{V}}} \mathbf{V}_{x_k}^h \right) \right) d\mathbf{x}\, dt + \epsilon}}, \tag{12b}$$

with $\epsilon := |K|^{\frac{1}{2}} (\Delta t^n)^{\frac{-1}{2}} \left(\frac{h}{\mathrm{diam}(\Omega)} \right)^{\theta}$ and $\theta \geq 1/2$ (chosen as 1) and

$$\overline{\mathrm{Res}}_{n,K} := \sqrt{\int_{I^n}\int_K \mathrm{Res} \cdot \left(\mathbf{U}_{\mathbf{V}}^{-1}(\mathbf{V}^h) \mathrm{Res} \right) d\mathbf{x}\, dt}. \tag{12c}$$

Here, C^{SC} is a positive constant, typically taken to be 1. We note that in the original formulation of the shock-capturing term [20, 19] both an inner residual term (defined by (12c)) and a boundary residual term enter the formula (12b). As the boundary residual term has only little influence, we do not include this term in our extension to the compressible Navier-Stokes equations and therefore do not present this term here.

2.3. Entropy stability for nonlinear systems

The design of the streamline diffusion (SD) shock-capturing (SC) discontinuous Galerkin (DG) scheme (4) is motivated by the consideration that it has to be entropy-stable for a generic nonlinear system of conservation laws, equipped with an entropy formulation. There holds the following theorem.

Theorem 2.1 (Partial restatement of Theorem 3.1 in [20])**.** *Consider the system of conservation laws* (1) *with a uniformly convex entropy function S and entropy flux functions Q^k ($1 \leq k \leq 2$). For simplicity, assume that the exact and approximate solutions have compact support inside the spatial domain Ω. Let the final time be denoted by t^N. Then, the streamline diffusion shock-capturing discontinuous Galerkin scheme* (4) *approximating* (1) *is entropy-stable, i.e., the approximate solutions satisfy*

$$\int_\Omega S(\mathbf{U}(\mathbf{V}_{N,-}^h(\mathbf{x})))\, d\mathbf{x} \leq \int_\Omega S(\mathbf{U}(\mathbf{V}_{0,-}^h(\mathbf{x})))\, d\mathbf{x}. \tag{13}$$

One can also extract the following property of the quasilinear form $\mathcal{B}_{\mathrm{DG}}$ from the proof of Theorem 2.1 (given as proof of Theorem 3.1 in [20]).

Lemma 2.1. *Under the conditions of Theorem 2.1, there holds*

$$\mathcal{B}_{\mathrm{DG}}(\mathbf{V}^h, \mathbf{V}^h) \geq \int_\Omega S(\mathbf{U}(\mathbf{V}_{N,-}^h(\mathbf{x})))\, d\mathbf{x} - \int_\Omega S(\mathbf{U}(\mathbf{V}_{0,-}^h(\mathbf{x})))\, d\mathbf{x}. \tag{14}$$

3. The compressible Navier-Stokes equations

The compressible Navier-Stokes equations in two space dimensions are given by

$$\mathbf{U}_t + \mathbf{F}^1(\mathbf{U})_{x_1} + \mathbf{F}^2(\mathbf{U})_{x_2} = \mathbf{H}^1(\mathbf{U})_{x_1} + \mathbf{H}^2(\mathbf{U})_{x_2}, \tag{15}$$

with

$$\mathbf{U} = \begin{bmatrix} \rho \\ \rho u \\ \rho v \\ E \end{bmatrix}, \quad \mathbf{F}^1(\mathbf{U}) = \begin{bmatrix} \rho u \\ \rho u^2 + p \\ \rho uv \\ u(E+p) \end{bmatrix}, \quad \mathbf{F}^2(\mathbf{U}) = \begin{bmatrix} \rho v \\ \rho uv \\ \rho v^2 + p \\ v(E+p) \end{bmatrix},$$

and

$$\mathbf{H}^1(\mathbf{U}) = \begin{bmatrix} 0 \\ \tau_{11} \\ \tau_{21} \\ \tau_{11}u + \tau_{12}v + \kappa\theta_{x_1} \end{bmatrix}, \quad \mathbf{H}^2(\mathbf{U}) = \begin{bmatrix} 0 \\ \tau_{12} \\ \tau_{22} \\ \tau_{21}u + \tau_{22}v + \kappa\theta_{x_2} \end{bmatrix}.$$

Here, $\rho = \rho(\mathbf{x}, t) > 0$ denotes the density, $u = u(\mathbf{x}, t)$ the velocity in x_1-direction, $v = v(\mathbf{x}, t)$ the velocity in x_2-direction, $p = p(\mathbf{x}, t) > 0$ the pressure, and

$$E = \frac{p}{\gamma - 1} + \frac{1}{2}\rho(u^2 + v^2)$$

the total energy with $\gamma > 1$ being the adiabatic constant. Additionally, $R > 0$ is the gas constant, $C_v > 0$ is the specific heat at constant volume, and $\theta = \frac{p}{R\rho} > 0$ refers to the temperature. The viscous stress tensor τ is given by

$$\tau = \mu \left(\nabla \begin{pmatrix} u \\ v \end{pmatrix} + \left(\nabla \begin{pmatrix} u \\ v \end{pmatrix} \right)^T \right) + \lambda \nabla \cdot \begin{pmatrix} u \\ v \end{pmatrix} \mathbb{I},$$

with superscript T denoting the transpose. We assume the viscosity parameters (μ, λ) and the conductivity $\kappa > 0$ to be constant. We use $\lambda = -\frac{2}{3}\mu$. We further assume the relation between μ and κ/R to be given by the Prandtl number $\mathrm{Pr} = 4\gamma/(9\gamma - 5)$ via

$$\frac{\kappa}{R} = \frac{\gamma C_v \mu}{R\mathrm{Pr}} = \frac{\gamma}{(\gamma - 1)\mathrm{Pr}}\mu.$$

In order to write the compressible Navier-Stokes equations in the form

$$\mathbf{U}_t + \nabla \cdot \begin{bmatrix} \mathbf{F}^1(\mathbf{U}) \\ \mathbf{F}^2(\mathbf{U}) \end{bmatrix} = \nabla \cdot \left(\begin{bmatrix} \mathbf{D}_{11}(\mathbf{U}) & \mathbf{D}_{12}(\mathbf{U}) \\ \mathbf{D}_{21}(\mathbf{U}) & \mathbf{D}_{22}(\mathbf{U}) \end{bmatrix} \begin{bmatrix} \mathbf{U}_{x_1} \\ \mathbf{U}_{x_2} \end{bmatrix} \right), \tag{16}$$

one needs to define suitable matrices $\mathbf{D}_{ij}(\mathbf{U}), i, j = 1, 2$. We do not give the specifics here (we refer the interested reader to [15]). We emphasize that the resulting matrix $\mathbf{D} = (\mathbf{D}_{ij})_{i,j=1,2}$ (which is formulated with respect to the conserved variables) is *not* symmetric.

Therefore, we rewrite (16) using entropy variables as degrees of freedom. For the transformation to entropy variables, we use the physical entropy and the corresponding entropy flux in the following way

$$S = -\frac{\rho s}{\gamma - 1}, \quad Q^1 = -\frac{\rho u s}{\gamma - 1}, \quad Q^2 = -\frac{\rho v s}{\gamma - 1}, \quad s = \log(p) - \gamma \log(\rho). \tag{17}$$

This results in the entropy variables (written in terms of primitive variables and s for simplicity)

$$\mathbf{V} = \left(\frac{\gamma - s}{\gamma - 1} - \frac{\rho(u^2 + v^2)}{2p}, \quad \frac{\rho u}{p}, \quad \frac{\rho v}{p}, \quad -\frac{\rho}{p} \right)^T. \tag{18}$$

Then, we can reformulate the compressible Navier-Stokes equations (15) in entropy variables as follows

$$\mathbf{U}(\mathbf{V})_t + \nabla \cdot \begin{bmatrix} \mathbf{F}^1(\mathbf{V}) \\ \mathbf{F}^2(\mathbf{V}) \end{bmatrix} = \nabla \cdot \left(\begin{bmatrix} \mathbf{A}_{11}(\mathbf{V}) & \mathbf{A}_{12}(\mathbf{V}) \\ \mathbf{A}_{21}(\mathbf{V}) & \mathbf{A}_{22}(\mathbf{V}) \end{bmatrix} \begin{bmatrix} \mathbf{V}_{x_1} \\ \mathbf{V}_{x_2} \end{bmatrix} \right), \tag{19}$$

with

$$\begin{aligned} \mathbf{A}(\mathbf{V}) &= \begin{bmatrix} \mathbf{A}_{11}(\mathbf{V}) & \mathbf{A}_{12}(\mathbf{V}) \\ \mathbf{A}_{21}(\mathbf{V}) & \mathbf{A}_{22}(\mathbf{V}) \end{bmatrix} \\ &= \frac{\mu}{v_4^3} \begin{bmatrix} 0 & 0 & 0 & 0 & 0 & 0 & 0 & 0 \\ 0 & -\frac{4}{3}v_4^2 & 0 & \frac{4}{3}v_2v_4 & 0 & 0 & \frac{2}{3}v_4^2 & -\frac{2}{3}v_3v_4 \\ 0 & 0 & -v_4^2 & v_3v_4 & 0 & -v_4^2 & 0 & v_2v_4 \\ 0 & \frac{4}{3}v_2v_4 & v_3v_4 & -\frac{4}{3}v_2^2 - v_3^2 + \chi v_4 & 0 & v_3v_4 & -\frac{2}{3}v_2v_4 & -\frac{1}{3}v_2v_3 \\ 0 & 0 & 0 & 0 & 0 & 0 & 0 & 0 \\ 0 & 0 & -v_4^2 & v_3v_4 & 0 & -v_4^2 & 0 & v_2v_4 \\ 0 & \frac{2}{3}v_4^2 & 0 & -\frac{2}{3}v_2v_4 & 0 & 0 & -\frac{4}{3}v_4^2 & \frac{4}{3}v_3v_4 \\ 0 & -\frac{2}{3}v_3v_4 & v_2v_4 & -\frac{1}{3}v_2v_3 & 0 & v_2v_4 & \frac{4}{3}v_3v_4 & -\frac{4}{3}v_3^2 - v_2^2 + \chi v_4 \end{bmatrix} \end{aligned} \tag{20}$$

and $\chi = \frac{\gamma}{(\gamma-1)\mathrm{Pr}}$. The matrix $\mathbf{A}$ has the following property [21].

Lemma 3.1. *The matrix* $\mathbf{A} \in \mathbb{R}^{8\times 8}$ *given in* (20) *is* symmetric positive semi-definite.

In the following lemma, we examine $\mathbf{A}$ further.

Lemma 3.2. *Let the matrix* $\mathbf{R} \in \mathbb{R}^{5\times 8}$ *be given by*

$$\mathbf{R} = \begin{pmatrix} 0 & 1 & 0 & 0 & 0 & 0 & 0 & 0 \\ 0 & 0 & \frac{1}{\sqrt{2}} & 0 & 0 & \frac{1}{\sqrt{2}} & 0 & 0 \\ 0 & 0 & 0 & 1 & 0 & 0 & 0 & 0 \\ 0 & 0 & 0 & 0 & 0 & 0 & 1 & 0 \\ 0 & 0 & 0 & 0 & 0 & 0 & 0 & 1 \end{pmatrix}. \tag{21}$$

Define

$$\hat{\mathbf{A}} = \mathbf{R}\mathbf{A}\mathbf{R}^T. \tag{22}$$

There holds:

(i) The matrix $\hat{\mathbf{A}} \in \mathbb{R}^{5\times 5}$ *is given by*

$$\hat{\mathbf{A}} = \begin{pmatrix} a_{22} & \sqrt{2}a_{23} & a_{24} & a_{27} & a_{28} \\ \sqrt{2}a_{32} & 2a_{33} & \sqrt{2}a_{34} & \sqrt{2}a_{37} & \sqrt{2}a_{38} \\ a_{42} & \sqrt{2}a_{43} & a_{44} & a_{47} & a_{48} \\ a_{72} & \sqrt{2}a_{73} & a_{74} & a_{77} & a_{78} \\ a_{82} & \sqrt{2}a_{83} & a_{84} & a_{87} & a_{88} \end{pmatrix}$$

and there holds

$$\mathbf{A} = \mathbf{R}^T \hat{\mathbf{A}} \mathbf{R}.$$

(ii) The matrix $\hat{\mathbf{A}}$ *is symmetric* positive definite *for* $\mu, \kappa > 0$.

(iii) Let $\mathrm{EV}(\mathbf{A})$ *denote the set of eigenvalues of the matrix* $\mathbf{A}$*. Then,*

$$\mathrm{EV}(\mathbf{A}) = \mathrm{EV}(\hat{\mathbf{A}}) \cup \{0\}$$

with the dimension of the eigenspace corresponding to the eigenvalue 0 *being 3.*

Proof. (i) Follows by direct computation, exploiting that columns 3 and 6 and rows 3 and 6, respectively, have the same entries.

(ii) Follows by direct computation, e.g., by verifying that all leading principal minors are positive.

(iii) Define

$$\mathbf{R}_{ext} = \begin{pmatrix} 0 & 1 & 0 & 0 & 0 & 0 & 0 & 0 \\ 0 & 0 & \frac{1}{\sqrt{2}} & 0 & 0 & \frac{1}{\sqrt{2}} & 0 & 0 \\ 0 & 0 & 0 & 1 & 0 & 0 & 0 & 0 \\ 0 & 0 & 0 & 0 & 0 & 0 & 1 & 0 \\ 0 & 0 & 0 & 0 & 0 & 0 & 0 & 1 \\ 0 & 0 & \frac{1}{\sqrt{2}} & 0 & 0 & -\frac{1}{\sqrt{2}} & 0 & 0 \\ 1 & 0 & 0 & 0 & 0 & 0 & 0 & 0 \\ 0 & 0 & 0 & 0 & 1 & 0 & 0 & 0 \end{pmatrix}.$$

Note that $\mathbf{R}_{ext}$ is an orthogonal matrix and that

$$\mathbf{R}_{ext}\mathbf{A}\mathbf{R}_{ext}^T = \begin{pmatrix} \hat{\mathbf{A}} & & & \\ & 0 & & \\ & & 0 & \\ & & & 0 \end{pmatrix}.$$

This directly implies the claim.

□

In section 5, we will prove entropy stability for the ST-SDSC-SIPG method for the compressible Navier-Stokes equations. To do so, we will need the quotient of the largest and smallest eigenvalue of $\hat{\mathbf{A}}(\mathbf{V}^h)$ to be uniformly bounded. We can derive this property from the following assumption which requires uniform boundedness of the computed solution.

Assumption 3.1 (Ass. for ST-SDSC-SIPG)**.** *We assume that there are uniform lower bounds* $\rho_0 > 0, p_0 > 0$ *such that* $\rho^h \geq \rho_0$ *and* $p^h \geq p_0$*. We further assume that there are uniform upper bounds* $\rho_M, u_M, v_M, p_M > 0$ *such that* $\rho^h \leq \rho_M$*,* $|u^h| \leq u_M$*,* $|v^h| \leq v_M$*, and* $p^h \leq p_M$*.*

Lemma 3.3. *Under Assumption 3.1, there exist bounds* λ *and* Λ *such that* $0 < \lambda \leq \lambda_1^h \leq \ldots \leq \lambda_5^h \leq \Lambda$*, where* λ_i^h *are the eigenvalues of* $\hat{\mathbf{A}}(\mathbf{V}^h)$ *(with* $\mathbf{V}^h$ *denoting the discrete solution).*

Proof. Under the Assumption 3.1, the entropy variables $|V_2^h|$,$|V_3^h|$,$|V_4^h|$ are uniformly bounded from above. In addition, $|V_4^h| = |\frac{\rho^h}{p^h}| \geq \frac{\rho_0}{p_M} > 0$. Thus, all the entries in $\mathbf{A}(\mathbf{V}^h)$ as well as in $\hat{\mathbf{A}}(\mathbf{V}^h)$ are bounded. This directly leads to an upper bound on the largest eigenvalue

$$C \geq \sum_{i,j}(a_{i,j})^2 = \mathrm{tr}(\mathbf{A}^\top\mathbf{A}) = \mathrm{tr}(\hat{\mathbf{A}}^\top\hat{\mathbf{A}}) = \sum_i(\lambda_i^h)^2. \tag{23}$$

Let us denote the upper bound of the eigenvalues by Λ and assume that the eigenvalues are sorted $0 \leq \lambda_1^h \leq \ldots \leq \lambda_5^h$. Then we have

$$\lambda_1^h \geq \lambda_1^h \frac{\lambda_2^h}{\Lambda} \cdots \frac{\lambda_5^h}{\Lambda} = \frac{\det \hat{\mathbf{A}}(\mathbf{V}^h)}{\Lambda^4}. \tag{24}$$

A lengthy but direct calculation yields

$$\det \hat{\mathbf{A}}(\mathbf{V}^h) = \frac{8}{3}\frac{\kappa^2}{R^2}\mu^3 \left(\frac{p^h}{\rho^h}\right)^7. \tag{25}$$

This is bounded from below by Assumption 3.1 and therefore this establishes a lower bound on the eigenvalues. □

4. The ST-NIPG and the ST-SIPG method

In this section, we present our methods ST-SDSC-NIPG and ST-SDSC-SIPG for solving the compressible Navier-Stokes equations in two space dimensions. Related versions in one space dimension have been presented in [29]. In the following, we will focus on the description of the methods in the interior of the space domain Ω. Necessary modifications to account for boundary conditions are discussed in section 4.3.

4.1. The IP formulation

We introduce the following notation: $\mathcal{F}$ refers to the collection of all edges of the triangulation $\mathcal{T}$ with $\mathcal{F}_i$ referring to the collection of interior edges and $\mathcal{F}_\Gamma$ referring to the collection of boundary edges. For each edge $e \in \mathcal{F}_i$ we assign a unit normal $\nu_e = (\nu_e^1, \nu_e^2)^T$, e.g., to point from K^1 to K^2. For an edge $e \in \mathcal{F}_\Gamma$, ν_e is assumed to coincide with the exterior unit normal vector. We define the *average* and *jump* for an edge $e \in \mathcal{F}_i$ shared by triangles K^1 and K^2 by

$$\left\{\mathbf{V}^h\right\} = \frac{1}{2}\left(\mathbf{V}^h_{K^1,-} + \mathbf{V}^h_{K^2,-}\right) \quad \text{and} \quad \left[\mathbf{V}^h\right] = \mathbf{V}^h_{K^1,-} - \mathbf{V}^h_{K^2,-}.$$

For an edge $e \in \mathcal{F}_\Gamma$, which belongs to cell K, we define $\left\{\mathbf{V}^h\right\} = \left[\mathbf{V}^h\right] = \mathbf{V}^h_{K,-}$.

For both ST-SDSC-NIPG and ST-SDSC-SIPG, we seek the discrete solution $\mathbf{V}^h \in \mathcal{V}^k$ such that

$$\mathcal{B}_{\mathrm{DG}}(\mathbf{V}^h, \mathbf{\Phi}^h) + \mathcal{B}^{\mathrm{IP}}_{\mathrm{SD}}(\mathbf{V}^h, \mathbf{\Phi}^h) + \mathcal{B}^{\mathrm{IP}}_{\mathrm{SC}}(\mathbf{V}^h, \mathbf{\Phi}^h) + \mathcal{B}_{\mathrm{IP},\zeta}(\mathbf{V}^h, \mathbf{\Phi}^h) = 0 \quad \forall\, \mathbf{\Phi}^h \in \mathcal{V}^k. \tag{26}$$

Here $\mathcal{B}_{\mathrm{DG}}$ is given by (5); $\mathcal{B}^{\mathrm{IP}}_{\mathrm{SD}}$ and $\mathcal{B}^{\mathrm{IP}}_{\mathrm{SC}}$ are modifications of the streamline diffusion and shock-capturing terms, which will be described below. The form $\mathcal{B}_{\mathrm{IP},\zeta}$ represents the discretization

of the diffusion term and is given by

$$\begin{aligned}
\mathcal{B}_{\mathrm{IP},\zeta}(\mathbf{V}^h,\mathbf{\Phi}^h) = &\sum_{n,K}\int_{I_n}\int_K \left(\mathbf{A}(\mathbf{V}^h)\begin{pmatrix}\mathbf{V}^h_{x_1}\\ \mathbf{V}^h_{x_2}\end{pmatrix}\right)\cdot\begin{pmatrix}\mathbf{\Phi}^h_{x_1}\\ \mathbf{\Phi}^h_{x_2}\end{pmatrix} d\mathbf{x}\,dt \\
&-\sum_n\sum_{e\in\mathcal{F}_i}\int_{I_n}\int_e \left(\mathbf{A}(\{\mathbf{V}^h\})\begin{pmatrix}\{\mathbf{V}^h_{x_1}\}\\ \{\mathbf{V}^h_{x_2}\}\end{pmatrix}\right)\cdot\begin{pmatrix}[\mathbf{\Phi}^h]\nu_e^1\\ [\mathbf{\Phi}^h]\nu_e^2\end{pmatrix} d\sigma(\mathbf{x})\,dt \qquad \text{(B1)}\\
&+\zeta\sum_n\sum_{e\in\mathcal{F}_i}\int_{I_n}\int_e \left(\mathbf{A}(\{\mathbf{V}^h\})\begin{pmatrix}\{\mathbf{\Phi}^h_{x_1}\}\\ \{\mathbf{\Phi}^h_{x_2}\}\end{pmatrix}\right)\cdot\begin{pmatrix}[\mathbf{V}^h]\nu_e^1\\ [\mathbf{V}^h]\nu_e^2\end{pmatrix} d\sigma(\mathbf{x})\,dt \qquad \text{(B2)}\\
&+\sum_n\sum_{e\in\mathcal{F}_i}\int_{I^n}\int_e \frac{\sigma}{h_e}\left(\mathbf{A}(\{\mathbf{V}^h\})\begin{pmatrix}[\mathbf{V}^h]\nu_e^1\\ [\mathbf{V}^h]\nu_e^2\end{pmatrix}\right)\cdot\begin{pmatrix}[\mathbf{\Phi}^h]\nu_e^1\\ [\mathbf{\Phi}^h]\nu_e^2\end{pmatrix} d\sigma(\mathbf{x})\,dt \qquad \text{(B3)}\\
&+\sum_n\sum_{e\in\mathcal{F}_\Gamma}\mathcal{B}^{\Gamma,n,e}_{\mathrm{IP},\zeta}(\mathbf{V}^h,\mathbf{\Phi}^h),
\end{aligned} \tag{27}$$

with $\mathcal{B}^{\Gamma,n,e}_{\mathrm{IP},\zeta}(\mathbf{V}^h,\mathbf{\Phi}^h)$ modeling the behavior for boundary edges $e\in\mathcal{F}_\Gamma$ and time interval I^n. We will describe the details for Dirichlet boundary conditions and adiabatic solid wall boundary conditions in section 4.3. The parameter $\sigma>0$ represents a penalty parameter and h_e denotes the length of the edge that is integrated over. We note that the definition of $\mathcal{B}_{\mathrm{IP},\zeta}$ is independent of the choice of the direction of the normal ν_e.

Notation 4.1. *The method is called NIPG method for $\zeta=1$ and SIPG method for $\zeta=-1$.*

4.2. Streamline diffusion and shock-capturing operator

We adjust the streamline diffusion and shock-capturing terms in order to account for the presence of the diffusion term. Different to (10), the intra-element residual is now given by

$$\mathrm{Res}^{\mathrm{IP}} = \mathbf{U}(\mathbf{V}^h)_t + \sum_{k=1}^2 \mathbf{F}^k(\mathbf{V}^h)_{x_k} - \sum_{k=1}^2 \left(\mathbf{A}_{k,1}(\mathbf{V}^h)\,\mathbf{V}^h_{x_1} + \mathbf{A}_{k,2}(\mathbf{V}^h)\,\mathbf{V}^h_{x_2}\right)_{x_k}. \tag{28}$$

One could then define a shock-capturing term $\mathcal{B}^{\mathrm{IP}}_{\mathrm{SC}}$ without further changes (other than using $\mathrm{Res}^{\mathrm{IP}}$ in the definition of $\overline{\mathrm{Res}}_{n,K}$, cmp. (12c), instead of Res). For the streamline diffusion, one needs to make the following adjustment

$$\begin{aligned}
\mathcal{B}^{\mathrm{IP}}_{\mathrm{SD}}(\mathbf{V}^h,\mathbf{\Phi}^h) = \sum_{n,K}\int_{I_n}\int_K \Bigg(&\mathbf{U}_{\mathbf{V}}(\mathbf{V}^h)\mathbf{\Phi}^h_t + \sum_{k=1}^2 \mathbf{F}^k_{\mathbf{V}}(\mathbf{V}^h)\mathbf{\Phi}^h_{x_k} \\
&-\sum_{k=1}^2\left(\mathbf{A}_{k,1}(\mathbf{V}^h)\,\mathbf{\Phi}^h_{x_1} + \mathbf{A}_{k,2}(\mathbf{V}^h)\,\mathbf{\Phi}^h_{x_2}\right)_{x_k}\Bigg)\cdot\left(\mathbf{D}^{\mathrm{SD}}_{n,K}\,\mathrm{Res}^{\mathrm{IP}}\right)\,d\mathbf{x}\,dt.
\end{aligned} \tag{29}$$

This adjustment is necessary in order to ensure the entropy stability of the resulting method.

If we use these formulations of $\mathcal{B}^{\mathrm{IP}}_{\mathrm{SC}}$ and $\mathcal{B}^{\mathrm{IP}}_{\mathrm{SD}}$ in (26), we will observe suboptimal convergence rates of $O(h^k)$ for tests involving smooth flow (compare the corresponding one-dimensional results in [29]). This was not the case for the original scheme (4) for conservation laws when the artificial diffusion terms were included. We believe that this is due to the fact that now second-order derivatives enter the computation of the residual and therefore reduce the order

of convergence of the residual. In [16], Hartmann presents shock-capturing terms for the compressible Navier-Stokes equations. If we multiplied $\mathcal{B}_{\mathrm{SC}}^{\mathrm{IP}}$ (on a cell-wise level) with $h_K^{0.9}$, the shock-capturing terms would have certain similarities. However, in this case our resulting shock-capturing term would not reduce to the shock-capturing term for the compressible Euler equations if the physical diffusion is not sufficiently resolved; as a result, oscillations might not be sufficiently damped.

We therefore adjust the formulation of the streamline diffusion and shock-capturing term differently: In [20], the authors introduced a pressure scaling term in $\mathcal{B}_{\mathrm{SC}}$ in order to capture contact discontinuities for the compressible Euler equations more sharply: they changed the term $D_{n,K}^{\mathrm{SC}}$ in (12b) in the following way

$$D_{n,K}^{\mathrm{SC}} \to D_{n,K}^{\mathrm{SC}} \cdot D_{n,K}^{p} \tag{30}$$

with

$$D_{n,K}^{p} = h_K^2 \frac{\frac{1}{\Delta t^n}\frac{1}{|K|}\int_{I^n}\int_K \sqrt{\sum_{k=1}^{2} p_{x_k x_k}^2}\, dx\, dt}{\frac{1}{\Delta t^n}\frac{1}{|K|}\int_{I^n}\int_K p\, dx\, dt}. \tag{31}$$

The authors did not include this term in their formulation of $\mathcal{B}_{\mathrm{SC}}$ (for general systems of conservation laws) as this adjustment is specific to the compressible Euler equations. We will use this formulation in our method for the compressible Navier-Stokes equations. To be consistent, we also change the streamline diffusion term and scale $\mathbf{D}_{n,K}^{\mathrm{SD}}$ defined in (11) with $D_{n,K}^{p}$. We summarize our changes compared to the streamline diffusion and shock-capturing terms of the original scheme:

- use the definition of the cell-wise residual $\mathrm{Res}^{\mathrm{IP}}$ given by (28) (instead of Res given by (10)); also change this in the definition of $\overline{\mathrm{Res}}_{n,K}$ in (12c);
- use the definition of $\mathcal{B}_{\mathrm{SD}}^{\mathrm{IP}}$ given by (29) instead of $\mathcal{B}_{\mathrm{SD}}$ given by (9);
- multiply $D_{n,K}^{\mathrm{SC}}$ in (12b) and $\mathbf{D}_{n,K}^{\mathrm{SD}}$ in (11) with the pressure scaling term defined in (31):

$$D_{n,K}^{\mathrm{SC}} \to D_{n,K}^{\mathrm{SC}} \cdot D_{n,K}^{p} \quad \text{and} \quad \mathbf{D}_{n,K}^{\mathrm{SD}} \to \mathbf{D}_{n,K}^{\mathrm{SD}} \cdot D_{n,K}^{p}. \tag{32}$$

4.3. Boundary conditions

We now present the details of $\mathcal{B}_{\mathrm{IP},\zeta}^{\Gamma,n,e}$ for the case of Dirichlet and adiabatic solid wall boundary conditions. Let $e \in \mathcal{F}_\Gamma$ belong to a cell K and denote by ν_e the exterior unit normal of triangle K on edge e.

4.3.1. Dirichlet boundary conditions

For imposing the Dirichlet boundary conditions $\mathbf{U} = \mathbf{g}$ weakly on an edge $e \in \mathcal{F}_\Gamma$, the term $\mathcal{B}_{\mathrm{IP},\zeta}^{\Gamma,n,e}$ in (27) uses the following modified versions of (B1) – (B3) from (27):

$$\begin{aligned}
\mathcal{B}_{\mathrm{IP},\zeta}^{\Gamma,n,e}(\mathbf{V}^h,\mathbf{\Phi}^h) = &-\int_{I_n}\int_e \left(\mathbf{A}(S_{\mathbf{U}}(\mathbf{g}))\begin{pmatrix}\mathbf{V}^h_{x_1,K,-}\\ \mathbf{V}^h_{x_2,K,-}\end{pmatrix}\right)\cdot\begin{pmatrix}\mathbf{\Phi}^h_{K,-}\nu_e^1\\ \mathbf{\Phi}^h_{K,-}\nu_e^2\end{pmatrix} d\sigma(\mathbf{x})\, dt && \text{(B1}')\\
&+\zeta\int_{I_n}\int_e \left(\mathbf{A}(S_{\mathbf{U}}(\mathbf{g}))\begin{pmatrix}\mathbf{\Phi}^h_{x_1,K,-}\\ \mathbf{\Phi}^h_{x_2,K,-}\end{pmatrix}\right)\cdot\begin{pmatrix}(\mathbf{V}^h_{K,-}-S_{\mathbf{U}}(\mathbf{g}))\nu_e^1\\ (\mathbf{V}^h_{K,-}-S_{\mathbf{U}}(\mathbf{g}))\nu_e^2\end{pmatrix} d\sigma(\mathbf{x})\, dt && \text{(B2}')\\
&+\int_{I^n}\int_e \frac{\sigma}{h_e}\left(\mathbf{A}(S_{\mathbf{U}}(\mathbf{g}))\begin{pmatrix}(\mathbf{V}^h_{K,-}-S_{\mathbf{U}}(\mathbf{g}))\nu_e^1\\ (\mathbf{V}^h_{K,-}-S_{\mathbf{U}}(\mathbf{g}))\nu_e^2\end{pmatrix}\right)\cdot\begin{pmatrix}\mathbf{\Phi}^h_{K,-}\nu_e^1\\ \mathbf{\Phi}^h_{K,-}\nu_e^2\end{pmatrix} d\sigma(\mathbf{x})\, dt. && \text{(B3}')
\end{aligned}$$

4.3.2. Adiabatic solid wall boundary conditions

We enforce on $e \in \mathcal{F}_\Gamma$ the conditions

- $u = v = 0$ (no slip condition) and
- $\kappa \frac{\partial \theta}{\partial \nu_e} = 0$ (no heat flux condition).

To this end, we define (based on the function value $\mathbf{V}^h_{K,-}$ on the edge e) the vector

$$\mathbf{v}_\Gamma = \begin{pmatrix} 0, & 0, & 0, & v_{4,K_-} \end{pmatrix}^T.$$

(We note that the entry v_{1,K_-} will not play a role in the following.) Further, we define $\mathbf{A}^\mu(\mathbf{v}_\Gamma)$ as $\mathbf{A}(\mathbf{v}_\Gamma)$ but with the heat conduction terms $\frac{\mu\gamma}{(\gamma-1)\mathrm{Pr}} \frac{1}{v_4^2}$ in entries $(\mathbf{A}(\mathbf{v}_\Gamma))_{4,4}$ and $(\mathbf{A}(\mathbf{v}_\Gamma))_{8,8}$ being removed. Then, for $e \in \mathcal{F}_\Gamma$, the term $\mathcal{B}^{\Gamma,n,e}_{\mathrm{IP},\zeta}$ in (27) (which captures the appropriate modifications of (B1) − (B3)) is given by

$$\mathcal{B}^{\Gamma,n,e}_{\mathrm{IP},\zeta}(\mathbf{V}^h, \mathbf{\Phi}^h) = -\int_{I^n}\int_e \left(\mathbf{A}^\mu(\mathbf{v}_\Gamma)\begin{pmatrix}\mathbf{V}^h_{x_1,K,-}\\ \mathbf{V}^h_{x_2,K,-}\end{pmatrix}\right)\cdot\begin{pmatrix}\mathbf{\Phi}^h_{K,-}\nu^1_e\\ \mathbf{\Phi}^h_{K,-}\nu^2_e\end{pmatrix} d\sigma(\mathbf{x})\,dt \qquad \text{(B1}')$$

$$+\zeta\int_{I^n}\int_e \left(\mathbf{A}^\mu(\mathbf{v}_\Gamma)\begin{pmatrix}\mathbf{\Phi}^h_{x_1,K,-}\\ \mathbf{\Phi}^h_{x_2,K,-}\end{pmatrix}\right)\cdot\begin{pmatrix}(\mathbf{V}^h_{K,-}-\mathbf{v}_\Gamma)\nu^1_e\\ (\mathbf{V}^h_{K,-}-\mathbf{v}_\Gamma)\nu^2_e\end{pmatrix} d\sigma(\mathbf{x})\,dt \qquad \text{(B2}')$$

$$+\int_{I^n}\int_e \frac{\sigma}{h_e}\left(\mathbf{A}^\mu(\mathbf{v}_\Gamma)\begin{pmatrix}(\mathbf{V}^h_{K,-}-\mathbf{v}_\Gamma)\nu^1_e\\ (\mathbf{V}^h_{K,-}-\mathbf{v}_\Gamma)\nu^2_e\end{pmatrix}\right)\cdot\begin{pmatrix}\mathbf{\Phi}^h_{K,-}\nu^1_e\\ \mathbf{\Phi}^h_{K,-}\nu^2_e\end{pmatrix} d\sigma(\mathbf{x})\,dt. \qquad \text{(B3}')$$

We note that the vector $\mathbf{A}^\mu(\mathbf{v}_\Gamma)\mathbf{v}_\Gamma$ has only zero entries. We keep it though for consistency with the formulation for interior edges and Dirichlet boundary conditions.

5. Entropy stability

In this section, we examine under which conditions the suggested formulations of the ST-SDSC-NIPG and the ST-SDSC-SIPG method are entropy stable for the compressible Navier-Stokes equations. For now, we will focus on the case of both the discrete and the continuous solution having compact support. Details concerning the entropy conditions in the presence of adiabatic solid wall boundary conditions will be presented in section 5.1.

Theorem 5.1 (Entropy stability for ST-SDSC-NIPG)**.** *Consider the compressible Navier-Stokes equations* (15) *and let the entropy pair* (S, Q) *be given by* (17)*. For simplicity, assume that the exact and approximate solution have compact support inside the spatial domain* Ω*. Let the final time be denoted by* t_N*. Then, the approximate solutions generated by the scheme* (26) *with* $\zeta = 1$ *and* $\sigma > 0$ *satisfy*

$$\int_\Omega S(\mathbf{U}(\mathbf{V}^h_{N,-}(\mathbf{x})))\,d\mathbf{x} \le \int_\Omega S(\mathbf{U}(\mathbf{V}^h_{0,-}(\mathbf{x})))\,d\mathbf{x}.$$

Theorem 5.2 (Entropy stability for ST-SDSC-SIPG)**.** *Let Assumption 3.1 and the assumptions of Theorem 5.1 hold true. Then, the approximate solutions generated by the scheme* (26) *with* $\zeta = -1$ *satisfy*

$$\int_\Omega S(\mathbf{U}(\mathbf{V}^h_{N,-}(\mathbf{x})))\,d\mathbf{x} \le \int_\Omega S(\mathbf{U}(\mathbf{V}^h_{0,-}(\mathbf{x})))\,d\mathbf{x},$$

provided σ is chosen sufficiently large such that

$$\sigma \geq \frac{c_{\text{inv}}\Lambda}{2\lambda} \tag{33}$$

where λ, Λ are defined in Lemma 3.3 and the constant c_{inv} will be specified below in Lemma 5.4.

In order to prove these theorems, we need the following auxiliary results.

Lemma 5.1. *For the ST-SDSC-NIPG method, under the assumptions of Theorem 5.1, there holds*

$$\mathcal{B}_{\text{IP},1}(\mathbf{V}^h, \mathbf{V}^h) \geq 0.$$

Proof. By definition, there holds for $\mathbf{V}^h$ having compact support

$$\begin{aligned}
\mathcal{B}_{\text{IP},1}(\mathbf{V}^h, \mathbf{V}^h) = &\sum_{n,K} \int_{I_n} \int_K \left(\mathbf{A}(\mathbf{V}^h) \begin{pmatrix} \mathbf{V}^h_{x_1} \\ \mathbf{V}^h_{x_2} \end{pmatrix} \right) \cdot \begin{pmatrix} \mathbf{V}^h_{x_1} \\ \mathbf{V}^h_{x_2} \end{pmatrix} d\mathbf{x}\, dt \\
&- \sum_n \sum_{e \in \mathcal{F}_i} \int_{I_n} \int_e \left(\mathbf{A}(\{\mathbf{V}^h\}) \begin{pmatrix} \{\mathbf{V}^h_{x_1}\} \\ \{\mathbf{V}^h_{x_2}\} \end{pmatrix} \right) \cdot \begin{pmatrix} [\mathbf{V}^h]\nu^1_e \\ [\mathbf{V}^h]\nu^2_e \end{pmatrix} d\sigma(\mathbf{x})\, dt \\
&+ \sum_n \sum_{e \in \mathcal{F}_i} \int_{I^n} \int_e \left(\mathbf{A}(\{\mathbf{V}^h\}) \begin{pmatrix} \{\mathbf{V}^h_{x_1}\} \\ \{\mathbf{V}^h_{x_2}\} \end{pmatrix} \right) \cdot \begin{pmatrix} [\mathbf{V}^h]\nu^1_e \\ [\mathbf{V}^h]\nu^2_e \end{pmatrix} d\sigma(\mathbf{x})\, dt \\
&+ \sum_n \sum_{e \in \mathcal{F}_i} \int_{I^n} \int_e \frac{\sigma}{h_e} \left(\mathbf{A}(\{\mathbf{V}^h\}) \begin{pmatrix} [\mathbf{V}^h]\nu^1_e \\ [\mathbf{V}^h]\nu^2_e \end{pmatrix} \right) \cdot \begin{pmatrix} [\mathbf{V}^h]\nu^1_e \\ [\mathbf{V}^h]\nu^2_e \end{pmatrix} d\sigma(\mathbf{x})\, dt.
\end{aligned}$$

The terms in the second and third line cancel each other. As $\mathbf{A}$ is positive semi-definite according to Lemma 3.1 and $\sigma > 0$, the terms in the first and last line are non-negative. This implies the claim. □

Lemma 5.2. *For the ST-SDSC-SIPG method, under the assumptions of Theorem 5.2, there holds*

$$\mathcal{B}_{\text{IP},-1}(\mathbf{V}^h, \mathbf{V}^h) \geq 0.$$

The proof is fairly lengthy and given below. With these prerequisites, we first want to present the proof of Theorems 5.1 and 5.2 – keeping in mind that Lemma 5.2 still needs to be shown.

Proof of Theorems 5.1 and 5.2. Testing in (26) with $\mathbf{\Phi}^h = \mathbf{V}^h$ results in

$$\mathcal{B}_{\text{DG}}(\mathbf{V}^h, \mathbf{V}^h) + \mathcal{B}^{\text{IP}}_{\text{SD}}(\mathbf{V}^h, \mathbf{V}^h) + \mathcal{B}^{\text{IP}}_{\text{SC}}(\mathbf{V}^h, \mathbf{V}^h) + \mathcal{B}_{\text{IP},\zeta}(\mathbf{V}^h, \mathbf{V}^h) = 0.$$

We consider each of the four terms individually:

1. *Term $\mathcal{B}_{\text{DG}}(\mathbf{V}^h, \mathbf{V}^h)$*: According to Lemma 2.1, there holds

$$\mathcal{B}_{\text{DG}}(\mathbf{V}^h, \mathbf{V}^h) \geq \int_\Omega S(\mathbf{U}(\mathbf{V}^h_{N,-}(\mathbf{x})))\, d\mathbf{x} - \int_\Omega S(\mathbf{U}(\mathbf{V}^h_{0,-}(\mathbf{x})))\, d\mathbf{x}.$$

(The proof transfers directly from compressible Euler equations to compressible Navier-Stokes equations.)

2. *Term* $\mathcal{B}_{\mathrm{SD}}^{\mathrm{IP}}(\mathbf{V}^h, \mathbf{V}^h)$: *Claim*: There holds

$$\mathcal{B}_{\mathrm{SD}}^{\mathrm{IP}}(\mathbf{V}^h, \mathbf{V}^h) \geq 0.$$

Proof: We essentially follow the proof of Theorem 3.1 in [20]. Based on our new definition of the streamline diffusion term given by (29), there holds by chain rule

$$\mathcal{B}_{\mathrm{SD}}^{\mathrm{IP}}(\mathbf{V}^h, \mathbf{V}^h) = \sum_{n,K} \int_{I_n} \int_K \mathrm{Res}^{\mathrm{IP}} \cdot \left(\mathbf{D}_{n,K}^{SD} \, \mathrm{Res}^{\mathrm{IP}} \right) \, d\mathbf{x} \, dt.$$

With the definition of $\mathbf{D}_{n,K}^{SD}$ given by (32) and (11) and due the entropy S being strictly convex, this implies $\mathcal{B}_{\mathrm{SD}}^{\mathrm{IP}}(\mathbf{V}^h, \mathbf{V}^h) \geq 0$.

3. *Term* $\mathcal{B}_{\mathrm{SC}}^{\mathrm{IP}}(\mathbf{V}^h, \mathbf{V}^h)$: *Claim*: There holds

$$\mathcal{B}_{\mathrm{SC}}^{\mathrm{IP}}(\mathbf{V}^h, \mathbf{V}^h) \geq 0.$$

Proof: By definition (compare (12a) and section 4.2)

$$\begin{aligned}
&\mathcal{B}_{\mathrm{SC}}^{\mathrm{IP}}(\mathbf{V}^h, \mathbf{V}^h) \\
&= \sum_{n,K} \int_{I_n} \int_K D_{n,K}^{\mathrm{SC}} \left(\mathbf{V}_t^h \cdot \left(\mathbf{U}_{\mathbf{V}}(\tilde{\mathbf{V}}_{n,K}) \mathbf{V}_t^h \right) + \sum_{k=1}^{2} \frac{h_K^2}{(\Delta t^n)^2} \mathbf{V}_{x_k}^h \cdot \left(\mathbf{U}_{\mathbf{V}}(\tilde{\mathbf{V}}_{n,K}) \mathbf{V}_{x_k}^h \right) \right) d\mathbf{x} dt
\end{aligned}$$

with $D_{n,K}^{\mathrm{SC}}$ being given by (32) and (12b) but with $\overline{\mathrm{Res}}_{n,K}$ being based on $\mathrm{Res}^{\mathrm{IP}}$ instead of being based on Res. Due to the strict convexity of the entropy function S, both $\mathbf{U}_{\mathbf{V}}$ and $\mathbf{U}_{\mathbf{V}}^{-1}$ are strictly positive definite. This implies $D_{n,K}^{\mathrm{SC}} \geq 0$. This also directly implies $\mathcal{B}_{\mathrm{SC}}^{\mathrm{IP}}(\mathbf{V}^h, \mathbf{V}^h) \geq 0$.

4. *Term* $\mathcal{B}_{\mathrm{IP},\zeta}(\mathbf{V}^h, \mathbf{V}^h)$: Based on Lemmata 5.1 and 5.2 there holds for both the ST-SDSC-NIPG and the ST-SDSC-SIPG method (under the respective assumptions)

$$\mathcal{B}_{\mathrm{IP},\zeta}(\mathbf{V}^h, \mathbf{V}^h) \geq 0.$$

Summarizing the estimates for the four terms results in

$$\begin{aligned}
0 &= \mathcal{B}_{\mathrm{DG}}(\mathbf{V}^h, \mathbf{V}^h) + \mathcal{B}_{\mathrm{SD}}^{\mathrm{IP}}(\mathbf{V}^h, \mathbf{V}^h) + \mathcal{B}_{\mathrm{SC}}^{\mathrm{IP}}(\mathbf{V}^h, \mathbf{V}^h) + \mathcal{B}_{\mathrm{IP},\zeta}(\mathbf{V}^h, \mathbf{V}^h) \\
&\geq \int_\Omega S(\mathbf{U}(\mathbf{V}_{N,-}^h(\mathbf{x}))) \, d\mathbf{x} - \int_\Omega S(\mathbf{U}(\mathbf{V}_{0,-}^h(\mathbf{x}))) \, d\mathbf{x} + 0 + 0 + 0,
\end{aligned}$$

which implies the claim. □

This concludes the proof of entropy stability for ST-SDSC-NIPG. In order to show entropy stability for ST-SDSC-SIPG, it remains to prove Lemma 5.2. To do so, we need the following lemma.

Lemma 5.3. *Let the matrix* $\mathbf{C} : \mathbb{R}^m \to \mathbb{R}^m$ *be symmetric positive semi-definite. Then there holds for arbitrary vectors* $v, w \in \mathbb{R}^m$ *and* $\delta > 0$

$$2 w^T \mathbf{C} v \leq \delta w^T \mathbf{C} w + \frac{1}{\delta} v^T \mathbf{C} v.$$

Proof. The proof follows directly from

$$0 \leq \frac{1}{\delta}\left((\delta w - v)^T \mathbf{C}(\delta w - v)\right) = \delta w^T \mathbf{C} w - 2 w^T \mathbf{C} v + \frac{1}{\delta} v^T \mathbf{C} v.$$

□

In the proof of Lemma 5.2, we also need to apply the following inverse trace estimate [33, 38].

Lemma 5.4. *There holds for $p^h \in \mathcal{P}^k(K)$*

$$\int_{\partial K} p^h(\mathbf{x})^2 \, d\sigma(\mathbf{x}) \leq \frac{c_{\text{inv}}}{h_K} \int_K p^h(\mathbf{x})^2 d\mathbf{x}$$

with $c_{\text{inv}} = c\,k^2$ and with h_K denoting the diameter of the cell K.

We can now proceed to proving Lemma 5.2.

Proof of Lemma 5.2. We exploit that the solution has compact support and that therefore the contributions from edges $e \in \mathcal{F}_\Gamma$ drop out. For simplicity, we will just write $\sum_e$ in the following with the meaning of $\sum_{e \in \mathcal{F}_i}$. Using that $\mathbf{A}$ is symmetric, there holds

$$\begin{aligned}
\mathcal{B}_{\text{IP},-1}(\mathbf{V}^h, \mathbf{V}^h) = &\sum_{n,K} \int_{I_n} \int_K \begin{pmatrix} \mathbf{V}^h_{x_1} & \mathbf{V}^h_{x_2} \end{pmatrix} \mathbf{A}(\mathbf{V}^h) \begin{pmatrix} \mathbf{V}^h_{x_1} \\ \mathbf{V}^h_{x_2} \end{pmatrix} d\mathbf{x}\, dt \\
&- 2 \sum_{n,e} \int_{I_n} \int_e \begin{pmatrix} [\mathbf{V}^h]\nu^1_e & [\mathbf{V}^h]\nu^2_e \end{pmatrix} \mathbf{A}(\{\mathbf{V}^h\}) \begin{pmatrix} \{\mathbf{V}^h_{x_1}\} \\ \{\mathbf{V}^h_{x_2}\} \end{pmatrix} d\sigma(\mathbf{x})\, dt \\
&+ \sum_{n,e} \int_{I_n} \int_e \frac{\sigma}{h_e} \begin{pmatrix} [\mathbf{V}^h]\nu^1_e & [\mathbf{V}^h]\nu^2_e \end{pmatrix} \mathbf{A}(\{\mathbf{V}^h\}) \begin{pmatrix} [\mathbf{V}^h]\nu^1_e \\ [\mathbf{V}^h]\nu^2_e \end{pmatrix} d\sigma(\mathbf{x})\, dt.
\end{aligned}$$

Applying Lemma 5.3 with arbitrary $\delta > 0$ to the terms in the middle line gives

$$\begin{aligned}
&2 \begin{pmatrix} [\mathbf{V}^h]\nu^1_e & [\mathbf{V}^h]\nu^2_e \end{pmatrix} \mathbf{A}(\{\mathbf{V}^h\}) \begin{pmatrix} \{\mathbf{V}^h_{x_1}\} \\ \{\mathbf{V}^h_{x_2}\} \end{pmatrix} \\
&\leq \delta h_e \begin{pmatrix} \{\mathbf{V}^h_{x_1}\} & \{\mathbf{V}^h_{x_2}\} \end{pmatrix} \mathbf{A}(\{\mathbf{V}^h\}) \begin{pmatrix} \{\mathbf{V}^h_{x_1}\} \\ \{\mathbf{V}^h_{x_2}\} \end{pmatrix} + \frac{1}{\delta h_e} \begin{pmatrix} [\mathbf{V}^h]\nu^1_e & [\mathbf{V}^h]\nu^2_e \end{pmatrix} \mathbf{A}(\{\mathbf{V}^h\}) \begin{pmatrix} [\mathbf{V}^h]\nu^1_e \\ [\mathbf{V}^h]\nu^2_e \end{pmatrix}
\end{aligned}$$

with δ to be determined later. We note that for $\sigma \geq \frac{1}{\delta}$, the second term can trivially be bounded by the penalty term. Let us therefore focus on the first term. Applying Lemma 3.2 and using the therein defined matrices $\mathbf{R}$ and $\hat{\mathbf{A}}$ implies

$$\begin{aligned}
&\sum_{n,K} \int_{I_n} \int_K \begin{pmatrix} \mathbf{V}^h_{x_1} & \mathbf{V}^h_{x_2} \end{pmatrix} \mathbf{A}(\mathbf{V}^h) \begin{pmatrix} \mathbf{V}^h_{x_1} \\ \mathbf{V}^h_{x_2} \end{pmatrix} d\mathbf{x}\, dt \\
&\quad - \sum_{n,e} \int_{I_n} \int_e \delta h_e \begin{pmatrix} \{\mathbf{V}^h_{x_1}\} & \{\mathbf{V}^h_{x_2}\} \end{pmatrix} \mathbf{A}(\{\mathbf{V}^h\}) \begin{pmatrix} \{\mathbf{V}^h_{x_1}\} \\ \{\mathbf{V}^h_{x_2}\} \end{pmatrix} d\sigma(\mathbf{x})\, dt \\
&= \sum_{n,K} \int_{I_n} \int_K \begin{pmatrix} \mathbf{V}^h_{x_1} & \mathbf{V}^h_{x_2} \end{pmatrix} \mathbf{R}^T \hat{\mathbf{A}}(\mathbf{V}^h) \mathbf{R} \begin{pmatrix} \mathbf{V}^h_{x_1} \\ \mathbf{V}^h_{x_2} \end{pmatrix} d\mathbf{x}\, dt \\
&\quad - \sum_{n,e} \int_{I_n} \int_e \delta h_e \begin{pmatrix} \{\mathbf{V}^h_{x_1}\} & \{\mathbf{V}^h_{x_2}\} \end{pmatrix} \mathbf{R}^T \hat{\mathbf{A}}(\{\mathbf{V}^h\}) \mathbf{R} \begin{pmatrix} \{\mathbf{V}^h_{x_1}\} \\ \{\mathbf{V}^h_{x_2}\} \end{pmatrix} d\sigma(\mathbf{x})\, dt.
\end{aligned}$$

We note that $\hat{\mathbf{A}}$ is positive definite and that by Assumption 3.1 its eigenvalues are uniformly bounded. Therefore, the above term can be bounded from below by

$$
\begin{aligned}
&\sum_{n,K}\int_{I_n}\int_K \lambda \begin{pmatrix}\mathbf{V}^h_{x_1} & \mathbf{V}^h_{x_2}\end{pmatrix}\mathbf{R}^T\mathbf{R}\begin{pmatrix}\mathbf{V}^h_{x_1}\\ \mathbf{V}^h_{x_2}\end{pmatrix} d\mathbf{x}\,dt\\
&-\sum_{n,e}\int_{I_n}\int_e \Lambda\delta h_e \begin{pmatrix}\{\mathbf{V}^h_{x_1}\} & \{\mathbf{V}^h_{x_2}\}\end{pmatrix}\mathbf{R}^T\mathbf{R}\begin{pmatrix}\{\mathbf{V}^h_{x_1}\}\\ \{\mathbf{V}^h_{x_2}\}\end{pmatrix} d\sigma(\mathbf{x})\,dt\\
&=\sum_{n,K}\int_{I_n}\int_K \lambda\left((v_2)^2_{x_1}+\frac{1}{2}\left((v_3)_{x_1}+(v_2)_{x_2}\right)^2+(v_4)^2_{x_1}+(v_3)^2_{x_2}+(v_4)^2_{x_2}\right) d\mathbf{x}\,dt\\
&-\sum_{n,e}\int_{I_n}\int_e \Lambda\delta h_e\left(\{(v_2)_{x_1}\}^2+\frac{1}{2}\left(\{(v_3)_{x_1}\}+\{(v_2)_{x_2}\}\right)^2+\{(v_3)_{x_2}\}^2+\sum_{k=1}^{2}\{(v_4)_{x_k}\}^2\right) d\sigma(\mathbf{x})\,dt.
\end{aligned}
$$

We want to transform the boundary integral to a domain integral. Let e be the edge between cells K^1 and K^2 and note that

$$
\{(v_j)_{x_d}\}^2_e=\left(\frac{1}{2}((v_j)_{x_d,K^1_-}+(v_j)_{x_d,K^2_-})\right)^2\le\frac{1}{2}\left((v_j)^2_{x_d,K^1_-}+(v_j)^2_{x_d,K^2_-}\right). \tag{34}
$$

Denote by e^1_K, e^2_K, and e^3_K the three edges of a triangle K. Further note that for fixed t $(v_j)_{x_d}(t,x_1,x_2)$ is a polynomial of degree $k-1$ in (x_1,x_2). We can apply the inverse trace estimate from Lemma 5.4 to get

$$
\sum_{k=1}^{3}\int_{e^k_K}(v_j)^2_{x_d,K_-}\,d\sigma(\mathbf{x})=\int_{\partial K}(v_j)^2_{x_d,K_-}\,d\sigma(\mathbf{x})\le\frac{c_{\text{inv}}}{h_K}\int_K(v_j)^2_{x_d}\,d\mathbf{x}.
$$

This implies

$$
\begin{aligned}
&\sum_{n,e}\int_{I_n}\int_e \Lambda\delta h_e\left(\{(v_2)_{x_1}\}^2+\frac{1}{2}\left(\{(v_3)_{x_1}+(v_2)_{x_2}\}\right)^2+\{(v_3)_{x_2}\}^2+\sum_{k=1}^{2}\{(v_4)_{x_k}\}^2\right) d\sigma(\mathbf{x})\,dt\\
&\quad\le\sum_{n,e}\int_{I_n}\int_e \Lambda\delta h_e\left(\frac{1}{2}\left((v_2)^2_{x_1,K^1_-}+(v_2)^2_{x_1,K^2_-}\right)+\ldots+\frac{1}{2}\left((v_4)^2_{x_2,K^1_-}+(v_4)^2_{x_2,K^2_-}\right)\right) d\sigma(\mathbf{x})\,dt\\
&\quad=\sum_{n,K}\int_{I_n}\sum_{k=1}^{3}\int_{e^k_K}\frac{1}{2}\Lambda\delta h_{e^k_K}\left((v_2)^2_{x_1,K_-}+\ldots+(v_4)^2_{x_2,K_-}\right) d\sigma(\mathbf{x})\,dt\\
&\quad\le\sum_{n,K}\int_{I_n}\int_K\frac{1}{2}c_{\text{inv}}\Lambda\delta\frac{h_{e^k_K}}{h_K}\left((v_2)^2_{x_1}+\frac{1}{2}\left((v_3)_{x_1}+(v_2)_{x_2}\right)^2+(v_3)^2_{x_2}+\sum_{k=1}^{2}(v_4)^2_{x_k}\right) d\mathbf{x}\,dt,
\end{aligned}
$$

where we have reordered the sum over edges as sum over triangles and have ignored contributions from the domain boundary Γ. As the length of each triangle edge $h_{e^k_K}$ can be bounded

by the diameter of the cell h_K, this implies

$$\begin{aligned}
&\sum_{n,K}\int_{I_n}\int_K \lambda \begin{pmatrix}\mathbf{V}^h_{x_1} & \mathbf{V}^h_{x_2}\end{pmatrix}\mathbf{R}^T\mathbf{R}\begin{pmatrix}\mathbf{V}^h_{x_1}\\ \mathbf{V}^h_{x_2}\end{pmatrix} d\mathbf{x}\,dt\\
&\quad -\sum_{n,e}\int_{I_n}\int_e \Lambda\delta h_e \begin{pmatrix}\{\mathbf{V}^h_{x_1}\} & \{\mathbf{V}^h_{x_2}\}\end{pmatrix}\mathbf{R}^T\mathbf{R}\begin{pmatrix}\{\mathbf{V}^h_{x_1}\}\\ \{\mathbf{V}^h_{x_2}\}\end{pmatrix} d\sigma(\mathbf{x})\,dt\\
&\geq \sum_{n,K}\int_{I_n}\int_K(\lambda-\frac{1}{2}c_{\text{inv}}\Lambda\delta)\left((v_2)^2_{x_1}+\frac{1}{2}\left((v_3)_{x_1}+(v_2)_{x_2}\right)^2+(v_3)^2_{x_2}+\sum_{k=1}^{2}(v_4)^2_{x_k}\right) d\mathbf{x}\,dt.
\end{aligned}$$

To summarize results, there holds

$$\begin{aligned}
&\mathcal{B}_{\text{IP},-1}(\mathbf{V}^h,\mathbf{V}^h)\\
&\geq \sum_{n,K}\int_{I_n}\int_K(\lambda-\frac{1}{2}c_{\text{inv}}\Lambda\delta)\left((v_2)^2_{x_1}+\frac{1}{2}\left((v_3)_{x_1}+(v_2)_{x_2}\right)^2+(v_3)^2_{x_2}+\sum_{k=1}^{2}(v_4)^2_{x_k}\right) d\mathbf{x}\,dt\\
&+\sum_{n,e}\int_{I_n}\int_e \frac{\sigma-\frac{1}{\delta}}{h_e}\begin{pmatrix}[\mathbf{V}^h]\nu^1_e & [\mathbf{V}^h]\nu^2_e\end{pmatrix}\mathbf{A}(\{\mathbf{V}^h\})\begin{pmatrix}[\mathbf{V}^h]\nu^1_e\\ [\mathbf{V}^h]\nu^2_e\end{pmatrix} d\sigma(\mathbf{x})\,dt,
\end{aligned}$$

which implies the claim if $\delta\leq\frac{2\lambda}{c_{\text{inv}}\Lambda}$ and $\sigma\geq\frac{1}{\delta}$, resulting in the condition $\sigma\geq\frac{c_{\text{inv}}\Lambda}{2\lambda}$, as given by (33). □

5.1. Boundary conditions

We now examine whether Theorems 5.1 and 5.2 still hold true in the presence of *adiabatic solid wall* boundary conditions, which are commonly used for the compressible Navier-Stokes equations. For these boundary conditions, there should hold

$$\frac{d}{dt}\int_\Omega S(\mathbf{U}(\mathbf{x},t))\,d\mathbf{x}\leq 0.$$

We assume the boundary of Ω to be split into parts Γ_{adia}, the part of the boundary on which we enforce adiabatic solid wall boundary conditions, and $\Gamma_{\text{remainder}}$, the remaining part of the boundary. We assume the two parts to be separated. We will ignore the boundary part $\Gamma_{\text{remainder}}$ by assuming compact support of the solution inside $\Omega\cup\Gamma_{\text{adia}}$. A classic application for this setup is flow around an airfoil (compare section 6.5), where Γ_{adia} corresponds to the airfoil boundary and $\Gamma_{\text{remainder}}$ corresponds to the far field boundary. There holds the following theorem.

Theorem 5.3 (Entropy stability for adiabatic solid wall boundary conditions)**.** *Consider the compressible Navier-Stokes equations. Let the assumptions of Theorems 5.1 and 5.2 hold true, but require $\sigma\geq\frac{c_{\text{inv}}\Lambda}{\lambda}$ for the ST-SDSC-SIPG method and only assume compact support of the solution inside $\Omega\cup\Gamma_{\text{adia}}$. For the numerical enforcement of boundary conditions on Γ_{adia} follow section 4.3.2 for the $\mathcal{B}_{\text{IP},\zeta}$-term and the description below for the $\mathcal{B}_{\text{DG}}$-term. Follow [22] for the definition of the entropy conservative flux $\mathbb{F}^{k,*}$ and use Rusanov diffusion for the operator $\mathbb{D}$. Then, the approximate solutions generated by the scheme* (26) *with $\zeta=1$ or $\zeta=-1$ satisfy*

$$\int_\Omega S(\mathbf{U}(\mathbf{V}^h_{N,-}(\mathbf{x})))\,d\mathbf{x}\leq\int_\Omega S(\mathbf{U}(\mathbf{V}^h_{0,-}(\mathbf{x})))\,d\mathbf{x}.$$

Like in the proof of Theorems 5.1 and 5.2, we again need to examine all four quasilinear forms appearing in (26): $\mathcal{B}_{\mathrm{DG}}$, $\mathcal{B}_{\mathrm{SD}}^{\mathrm{IP}}$, $\mathcal{B}_{\mathrm{SC}}^{\mathrm{IP}}$, and $\mathcal{B}_{\mathrm{IP},\zeta}$. Examining the definitions of the artificial diffusion terms $\mathcal{B}_{\mathrm{SD}}^{\mathrm{IP}}$ and $\mathcal{B}_{\mathrm{SC}}^{\mathrm{IP}}$, we find that only spacetime domain terms enter the formulation, no spatial boundary terms. Therefore, the proof of Theorems 5.1 and 5.2 directly transfers.

Next, we consider the term $\mathcal{B}_{\mathrm{DG}}$. In the proof for the case of compact support inside Ω, we referred to Lemma 2.1 (which is shown in Hiltebrand and Mishra [20]) for an estimate for this term. The same estimate as claimed in Lemma 2.1 can be shown for the case considered in Theorem 5.3. As the focus of this contribution is on the viscous terms, we provide the corresponding result as Lemma A.1 in appendix A. Here, we shortly describe how we enforce the boundary conditions: like for interior edges, we compute a numerical flux for edges on Γ_{adia}. One input argument is the state from the interior of the flow domain, denoted by $\mathbf{V}_{K,-}^h$. We define the other input argument for the numerical flux $\mathbb{F}$ as

$$\mathbf{V}_{K,+}^h = \begin{pmatrix} v_{1,K_-}^h, & -v_{2,K_-}^h, & -v_{3,K_-}^h, & v_{4,K_-}^h \end{pmatrix}^T. \tag{35}$$

This corresponds to inverting the velocity vector and ensures that the second and third component of $\frac{1}{2}\left(\mathbf{V}_{K,-}^h + \mathbf{V}_{K,+}^h\right)$ vanish.

Finally, we need to show (in the presence of adiabatic solid wall boundary conditions)

$$\mathcal{B}_{\mathrm{IP},\zeta}(\mathbf{V}^h, \mathbf{V}^h) \geq 0. \tag{36}$$

We will do that in the following by examining the special case of a cell K that has edges $e \in \mathcal{F}_{\Gamma_{\mathrm{adia}}}$, on which adiabatic solid wall boundary conditions are enforced.

5.1.1. ST-SDSC-NIPG

Let us focus on the case of a boundary edge $e \in \mathcal{F}_{\Gamma_{\mathrm{adia}}}$. There holds $\mathbf{A}^\mu(\mathbf{v}_\Gamma)\mathbf{v}_\Gamma = \mathbf{0}$. Therefore, due to the symmetry of $\mathbf{A}^\mu$, the boundary terms (B1′) and (B2′) in the definition of $\mathcal{B}_{\mathrm{IP},\zeta}^{\Gamma,n,e}$ cancel each other for $\zeta = 1$. Further, due to $\mathbf{A}^\mu$ being positive semi-definite, the term (B3′) is non-negative. Together with the considerations for interior edges, this implies (36).

5.1.2. ST-SDSC-SIPG

For interior edges $e \in \mathcal{F}_i$, we proceed as described in the proof of Lemma 5.2. Let us therefore focus on the boundary edge $e \in \mathcal{F}_{\Gamma_{\mathrm{adia}}}$. Different to the ST-SDSC-NIPG method, we need to include the domain term

$$\int_{I^n}\int_K \begin{pmatrix} \mathbf{V}_{x_1}^h & \mathbf{V}_{x_2}^h \end{pmatrix} \mathbf{A}(\mathbf{V}^h) \begin{pmatrix} \mathbf{V}_{x_1}^h \\ \mathbf{V}_{x_2}^h \end{pmatrix} d\mathbf{x}\, dt$$

in our considerations. Using $\mathbf{A}^\mu(\mathbf{v}_\Gamma)\mathbf{v}_\Gamma = \mathbf{0}$, we consider

$$\begin{aligned}
&\int_{I^n}\int_K \begin{pmatrix} \mathbf{V}_{x_1}^h & \mathbf{V}_{x_2}^h \end{pmatrix} \mathbf{A}(\mathbf{V}^h) \begin{pmatrix} \mathbf{V}_{x_1}^h \\ \mathbf{V}_{x_2}^h \end{pmatrix} d\mathbf{x}\, dt \\
-2&\int_{I^n}\int_e \begin{pmatrix} \mathbf{V}_{x_1,K,-}^h & \mathbf{V}_{x_2,K,-}^h \end{pmatrix} \mathbf{A}^\mu(\mathbf{v}_\Gamma) \begin{pmatrix} \mathbf{V}_{K,-}^h \nu_e^1 \\ \mathbf{V}_{K,-}^h \nu_e^2 \end{pmatrix} d\sigma(\mathbf{x})\, dt \\
+&\int_{I^n}\int_e \frac{\sigma}{h_e} \begin{pmatrix} \mathbf{V}_{K,-}^h \nu_e^1 & \mathbf{V}_{K,-}^h \nu_e^2 \end{pmatrix} \mathbf{A}^\mu(\mathbf{v}_\Gamma) \begin{pmatrix} \mathbf{V}_{K,-}^h \nu_e^1 \\ \mathbf{V}_{K,-}^h \nu_e^2 \end{pmatrix} d\sigma(\mathbf{x})\, dt.
\end{aligned}$$

We proceed as in the proof of Lemma 5.2 and apply Young's inequality to split the term in the middle line. Then, we bound one part by the penalty term. The other part can be bounded by the domain term following the proof of Lemma 5.2 (together with the boundary terms from interior edges). Note that we did not change the matrix occurring in the domain term. Therefore, we can bound this term from below using the lower bound for the eigenvalues λ provided Assumption 3.1 holds true. Note further that the eigenvalues of $\mathbf{A}^{\mu}(\mathbf{v}_{\Gamma})$ can still be bounded from above by Λ from Lemma 3.3.

Comparing with the proof of Lemma 5.2, we find that there is a factor of $\frac{1}{2}$ (which was present for interior edges, compare (34)) missing. Therefore, we need to increase the penalty parameter σ by a factor of 2 on boundary cells to guarantee entropy stability for adiabatic solid wall boundary conditions compared to the case considered in Theorem 5.2 .

6. Numerical results

In the following, we present numerical examples, mostly comparing with standard tests from the literature, to test our claims about high-order accuracy in smooth flow and robustness of the scheme. Following (8), the numerical flux $\mathbb{F}$ is split into two parts: We follow [22] for the definition of $\mathbb{F}^{k,*}$ (the entropy-conservative flux in x_k-direction) for the compressible Euler equations and use Rusanov diffusion for the operator $\mathbb{D}$ [20]. Also, we will slightly change our notation and use (x, y) to denote coordinates (instead of (x_1, x_2)) for our tests in two space dimensions. We will start with the Sod test in one space dimension in order to confirm the appropriate behavior of our artificial diffusion terms close to shocks and contact discontinuities.

In many test cases, the results for ST-SDSC-SIPG and ST-SDSC-NIPG are very similar to each other. We will therefore only present results for ST-SDSC-NIPG unless otherwise specified. We use $\sigma = 10$ and $\sigma = 20$ for our computations for ST-SDSC-NIPG and ST-SDSC-SIPG, respectively.

For our one-dimensional test, we use a uniform mesh. For our tests in two dimensions, we use a structured or unstructured triangle mesh in space. Although not needed for stability, we typically use for our time-dependent test problems a CFL condition with CFL number 0.5 (taken with respect to the convective part of the equations) for accuracy reasons.

6.1. Sod test in 1d

We start with a version of the Sod test, similar to the test in [37, 29]. Although the focus of this contribution is on 2d, we start with this 1d test problem as it is very well-understood and very suitable for testing the behavior of our artificial diffusion terms. We consider initial data

$$(\rho, m, E) = \begin{cases} (1.0, 0.0, 2.5) & \text{if} \quad x < 0, \\ (0.125, 0.0, 0.25) & \text{if} \quad x > 0, \end{cases}$$

on the domain $\Omega = (-0.5, 0.5)$. The viscosity $\nu = 2.5 \cdot 10^{-6}$ is fairly small.

Figure 1 shows the result for density for the final time $T = 0.2$ for polynomial degrees one, two, and three and for two different grid resolutions $h = 1.0 \cdot 10^{-2}$ and $h = 1.25 \cdot 10^{-4}$. Although we solved the compressible Navier-Stokes equations, the small diffusion terms could not be resolved on the coarse grid with mesh width $h = 1.0 \cdot 10^{-2}$ and therefore the solution behaves similar to the solution of the compressible Euler equations: we observe oscillations around contact discontinuity and shock when not using artificial viscosity terms. The oscillations are

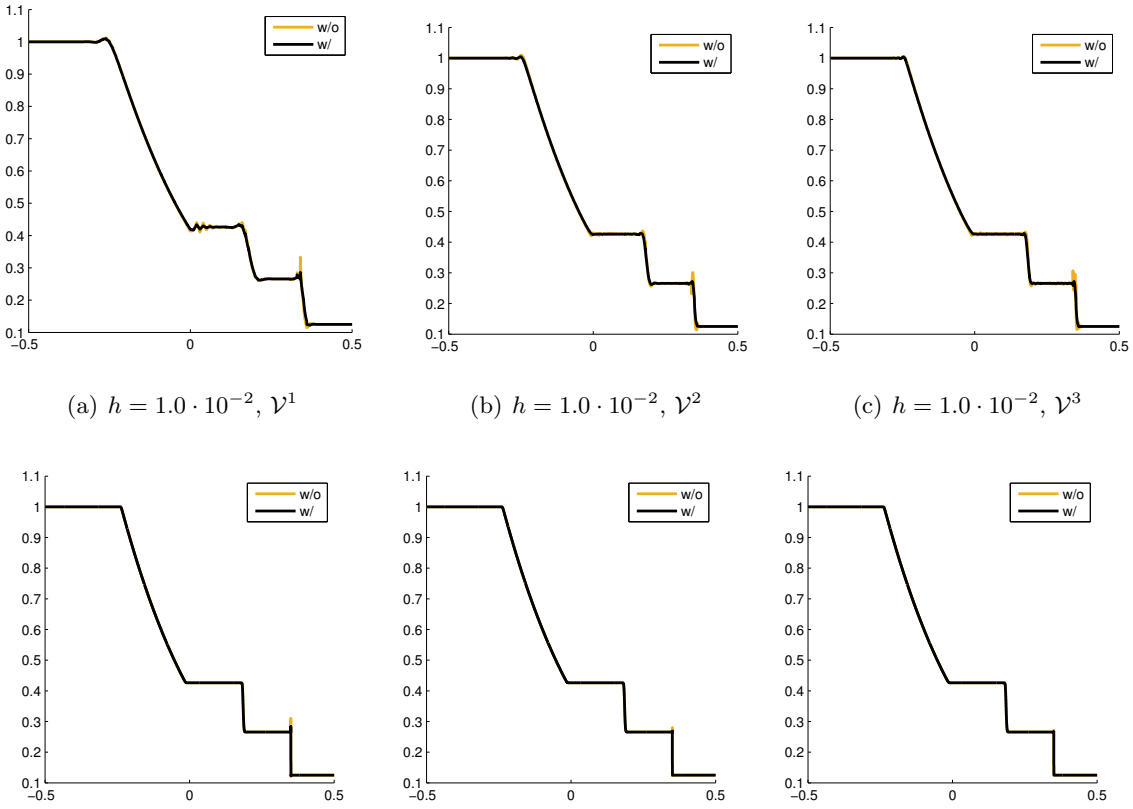

(a) $h = 1.0 \cdot 10^{-2}$, $\mathcal{V}^1$ (b) $h = 1.0 \cdot 10^{-2}$, $\mathcal{V}^2$ (c) $h = 1.0 \cdot 10^{-2}$, $\mathcal{V}^3$

(d) $h = 1.25 \cdot 10^{-4}$, $\mathcal{V}^1$ (e) $h = 1.25 \cdot 10^{-4}$, $\mathcal{V}^2$ (f) $h = 1.25 \cdot 10^{-4}$, $\mathcal{V}^3$

Figure 1: Sod test: Result for density for varying polynomial degree and grid resolution. The plots show the solution for using the methods both *without* $\mathcal{B}_{\mathrm{SD}}^{\mathrm{IP}}$ and $\mathcal{B}_{\mathrm{SC}}^{\mathrm{IP}}$ terms ('w/o') and *with* $\mathcal{B}_{\mathrm{SD}}^{\mathrm{IP}}$ and $\mathcal{B}_{\mathrm{SC}}^{\mathrm{IP}}$ terms ('w/').

mostly gone when the $\mathcal{B}_{\mathrm{SD}}^{\mathrm{IP}}$ and $\mathcal{B}_{\mathrm{SC}}^{\mathrm{IP}}$ terms included. This shows that (a) stabilization terms are needed in underresolved regions of the flow and (b) that our $\mathcal{B}_{\mathrm{SD}}^{\mathrm{IP}}$ and $\mathcal{B}_{\mathrm{SC}}^{\mathrm{IP}}$ terms are suitable for that purpose.

If we solve the compressible Navier-Stokes equations on a finer grid with width $h = 1.25 \cdot 10^{-4}$ the physical diffusion will serve as stabilization. We observe in Figure 1 that with increasing polynomial degree the overshoot decreases due to a better resolution of the physical diffusion. Thus artificial stabilization is not really needed. But the results also show that our artificial terms still slightly enhance the solution for this scenario.

6.2. Manufactured solution

To test the accuracy of our scheme in smooth flow we use the test of a manufactured solution provided in the literature [15] but we use a square domain $(-3, 3)^2$ without the cylinder cut out[1]. As our artificial diffusion terms are not meant to deal with source terms we do not include them in the simulation.

The results for the L^1 error over all 4 components at the final time $T = 0.1$ for $\nu = 0.01$ for ST-SDSC-SIPG and ST-SDSC-NIPG (without $\mathcal{B}_{\mathrm{SD}}^{\mathrm{IP}}$ and $\mathcal{B}_{\mathrm{SC}}^{\mathrm{IP}}$) are shown in Figure 2. We observe convergence rates of $O(h^{k+1})$ for all scenarios. Also, the actual errors for ST-SDSC-SIPG and ST-SDSC-NIPG are almost identical. We expected to see suboptimal convergence rates of $O(h^2)$ for ST-SDSC-NIPG for $\mathcal{V}^2$. We attribute the surprisingly good convergence rate to the fact that the test problem is too simple and uses $u = v = 1$.

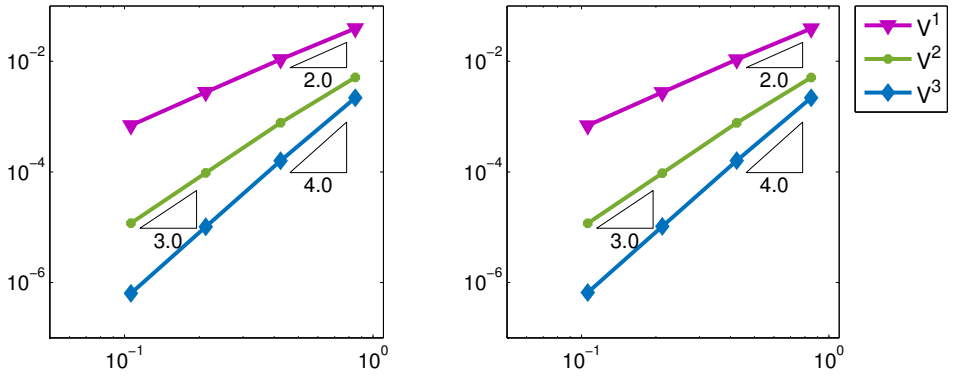

(a) ST-SIPG (b) ST-NIPG

Figure 2: Results for manufactured solution: L^1 error measured over all components. The x-axis denotes the mesh width h, the y-axis the L^1 error.

6.3. Steady state test with smooth solution

To be able to also include our artificial diffusion term, we construct a smooth solution of the compressible Navier-Stokes equations ourselves. We restrict ourselves to a steady state, axisymmetric case such that we are able to construct a reference solution by numerical integration of a system of ODEs. More precisely, consider the steady state compressible Navier-Stokes

[1]Note that there is a typo in [15, p. 276, eq (75)]: the term 3ω in s_2 and s_3 needs to be replaced by $3k$.

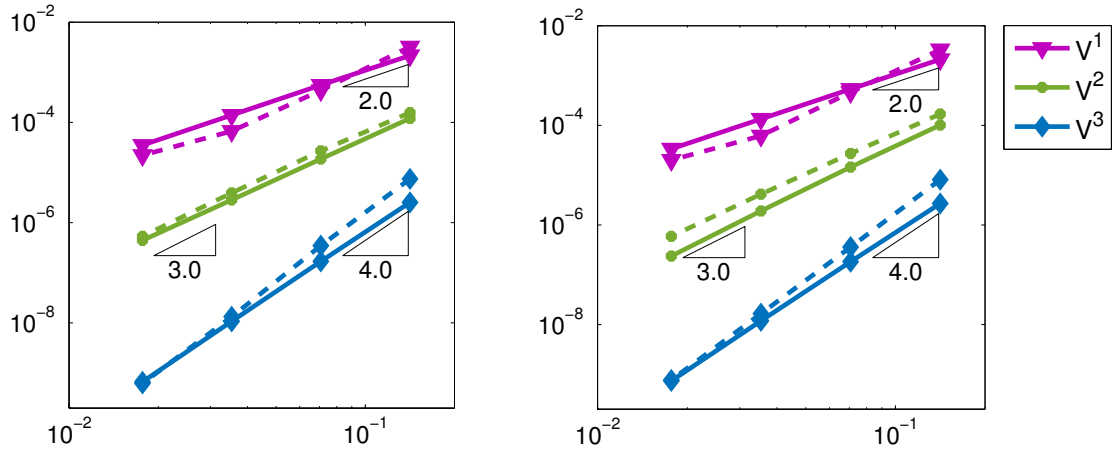

(a) ST-SDSC-SIPG (b) ST-SDSC-NIPG

Figure 3: Results for steady state test with smooth solution: L^1 error measured over all components. The x-axis denotes the mesh width h, the y-axis the L^1 error. Dashed lines correspond to results with $\mathcal{B}_{\mathrm{SD}}^{\mathrm{IP}}$ and $\mathcal{B}_{\mathrm{SC}}^{\mathrm{IP}}$, solid lines to results without $\mathcal{B}_{\mathrm{SD}}^{\mathrm{IP}}$ and $\mathcal{B}_{\mathrm{SC}}^{\mathrm{IP}}$.

equations in polar coordinates (r, ϕ) with velocity components u^r and u^ϕ. (In the following, superscripts r and ϕ denote the respective components of u, subscripts denote partial derivatives.) For simplicity, we set tangential velocity $u^\phi = 0$. This results in

$$\begin{aligned}(\rho u^r)_r &= -\frac{1}{r}\rho u^r \\ (\rho (u^r)^2 + p)_r &= -\frac{1}{r}\rho (u^r)^2 + \frac{1}{r}(r\tau^{rr})_r - \frac{1}{r}\tau^{\phi\phi} \\ (u^r(E+p))_r &= -\frac{1}{r}u^r(E+p) + \frac{1}{r}(r\tau^{rr}u^r)_r + \kappa\frac{1}{r}(r\theta_r)_r\end{aligned} \tag{37}$$

with

$$\tau^{rr} = (2\mu+\lambda)u_r^r + \lambda\frac{u^r}{r}, \quad \tau^{\phi\phi} = (2\mu+\lambda)\frac{u^r}{r} + \lambda u_r^r,$$
$$E = \frac{p}{\gamma-1} + \frac{1}{2}\rho(u^r)^2, \qquad \theta = \frac{p}{R\rho}.$$

Here, unknowns density ρ, radial velocity u^r, and pressure p are functions of the radius r only. We solve the first equation in (37) for ρ analytically using integration. We solve the remaining two equations with unknowns u^r and p numerically with high accuracy. We use the initial conditions $\rho(1) = 1$, $u^r(1) = 1$, $p(1) = 1$, $u_r^r(1) = 0.1$, and $p_r(1) = 0.1$ and parameter values $\mu = 2.5/\sqrt{10}$ and $\kappa/R = 1.1875 * \sqrt{10}$. We solve for $r \in [1, 3]$. We use the result as a reference solution that we compare our numerical solution with.

For our numerical test, we use the following data: the initial and boundary data are given by the reference solution, and we solve on the domain $(1/\sqrt{2}, 1+1/\sqrt{2})^2$ until we have reached steady state.

Figure 3 shows the L^1 error measured over all components for the ST-SDSC-SIPG and the ST-SDSC-NIPG scheme for both options of using the terms $\mathcal{B}_{\mathrm{SD}}^{\mathrm{IP}}$ and $\mathcal{B}_{\mathrm{SC}}^{\mathrm{IP}}$ (dashed line) and not using them (solid line). We essentially observe optimal convergence rates of $O(h^{k+1})$ for all scenarios. In particular,

- we do not observe a decay of convergence order for the ST-SDSC-NIPG scheme for $\mathcal{V}^2$;
- our artificial diffusion terms $\mathcal{B}_{\mathrm{SD}}^{\mathrm{IP}}$ and $\mathcal{B}_{\mathrm{SC}}^{\mathrm{IP}}$ do not deteriorate the convergence order of our scheme; also in terms of the actual size of the errors, the results with $\mathcal{B}_{\mathrm{SD}}^{\mathrm{IP}}$ and $\mathcal{B}_{\mathrm{SC}}^{\mathrm{IP}}$ are fairly close to the results without artificial diffusion terms; it is not clear why for $\mathcal{V}^1$ the solution with artificial diffusion shows smaller errors than without artificial diffusion; (for one grid level finer, the results with $\mathcal{B}_{\mathrm{SD}}^{\mathrm{IP}}$ and $\mathcal{B}_{\mathrm{SC}}^{\mathrm{IP}}$ are still slightly better than without $\mathcal{B}_{\mathrm{SD}}^{\mathrm{IP}}$ and $\mathcal{B}_{\mathrm{SC}}^{\mathrm{IP}}$ but the quotient is close to 1.)

6.4. Blasius boundary layer

Next, we consider the classic Blasius boundary layer test for low-speed laminar flow along an adiabatic plate. Under the assumptions that the flow is incompressible and that the Reynolds number is sufficiently large, one assumes the solution of the compressible Navier-Stokes equations in the boundary layer to be close to the solution of the Prandtl boundary layer equations that we want to compare our results with.

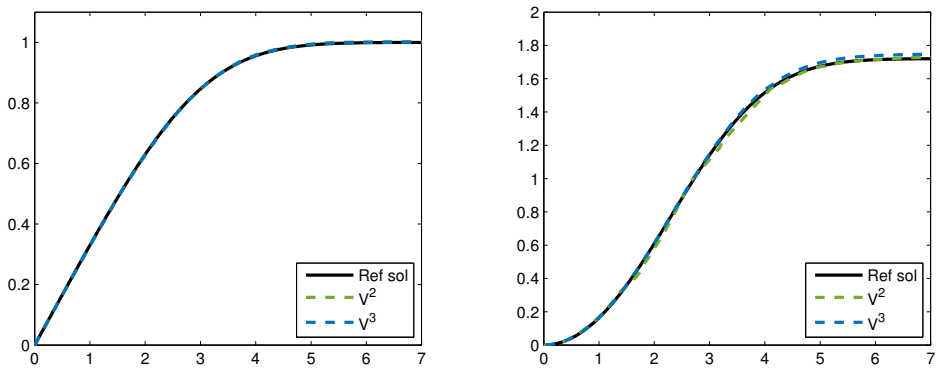

(a) η vs. $\tilde{u}$ (b) η vs. $\tilde{v}$

Figure 4: Results for Blasius boundary layer: scaled velocities $\tilde{u}$ and $\tilde{v}$.

We solve the compressible Navier-Stokes equations with Mach number $M = 0.1$, Reynolds number $\mathrm{Re} = 10^5$, and Prandtl number $\mathrm{Pr} = 0.72$. Our grid uses 2544 cells and is chosen such that there are sufficient cells in the boundary layer to resolve it. Therefore, we do not include artificial viscosity terms in this test. We solve on the domain $(-0.5, 1) \times (0, 0.25)$ and assume the flat plate to be located at $[0, 1] \times [0]$. We evaluate scaled velocities $\tilde{u}$ and $\tilde{v}$ at $x = 0.5$ and plot η vs. $\tilde{u}$ and η vs. $\tilde{v}$ with

$$\eta = \frac{y}{x}\sqrt{\mathrm{Re}_x}, \quad \mathrm{Re}_x = \frac{u_\infty x}{\nu}, \quad \tilde{u} = \frac{u}{u_\infty}, \quad \tilde{v} = \frac{2v}{u_\infty}\sqrt{\mathrm{Re}_x},$$

with u_∞ denoting the far field velocity in x-direction, which satisfies $\mathrm{Re} = \frac{u_\infty L}{\nu}$ with L denoting the plate length.

Figure 4 shows the results for the scaled velocities $\tilde{u}$ and $\tilde{v}$, both plotted against η, for polynomial degrees two and three. The results for $\tilde{u}$ match very well with the reference solution. Even for coarser grids, it was very straight-forward to capture the scaled u-velocity well. A

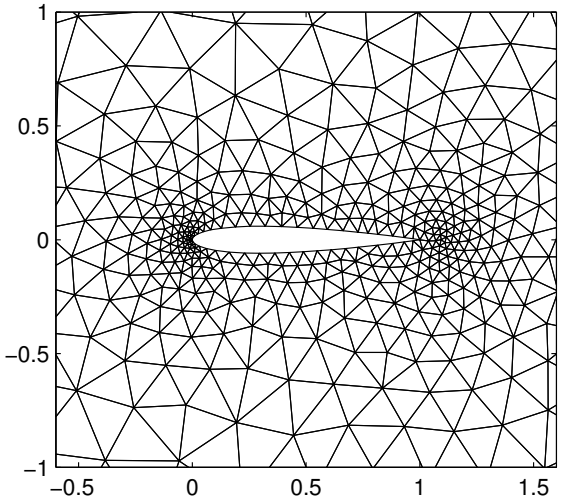

Figure 5: Airfoil test: Base mesh M with 1728 cells zoomed around the airfoil.

more challenging test is the approximation of the velocity $\tilde{v}$ – for which we also observe a good agreement with the 'analytic' solution. We notice the following though: as we compute the discrete solution more accurately, the agreement with the reference solution seems to become slightly worse, i.e., the computed solution then lies slightly above the reference solution. We attribute this to the fact that our reference solution is not the true solution of the compressible Navier-Stokes equations for the chosen setting – but for the boundary layer equations.

6.5. Flow around NACA 0012 airfoil

We conclude our numerical results with a standard test in the literature: flow around a two-dimensional NACA 0012 airfoil. We use the following airfoil geometry

$$y = \pm 0.594689181 \cdot \big[0.298222773\sqrt{x} - 0.127125232x \\ -0.357907906x^2 + 0.291984971x^3 - 0.105174606x^4\big] .$$

Our base mesh M has 1728 triangles and uses a far field radius of 50 chords. It has been generated using DistMesh [31]. Figure 5 shows the close neighborhood of the airfoil. We also use once and twice globally refined meshes, denoted by M1 and M2, with 6912 and 27648 cells, respectively. We note that the results of airfoil tests strongly depend on the quality of the mesh: the goal is to have enough cells in the boundary layer while having as little cells as possible in total. Our mesh has not been optimized in that respect. The focus here is on validation of our method, for which this mesh turned out to be sufficient. We use piecewise cubic polynomials for our tests and $\mathrm{Pr} = 0.72$. We use a higher-order boundary approximation along the airfoil boundary to be consistent with using higher-order polynomial spaces.

Table 1: Airfoil test: Results for Re=5000, Ma=0.5, $\alpha = 0°$.

	c_D^p	c_D^v	c_L^p	c_L^v
ST-SIPG, mesh M1	0.02409	0.03371	-3.33e-03	-1.22e-04
ST-NIPG, mesh M1	0.02385	0.03367	-3.38e-03	-1.05e-04
ST-SIPG, mesh M2	0.02231	0.03238	1.50e-04	1.31e-05
ST-NIPG, mesh M2	0.02229	0.03239	1.44e-04	1.28e-05
Hartmann & Houston [17]	0.02229	0.03254		
Swanson & Langer [35]	0.02279	0.03279		
Theory			0	0

6.5.1. Re=5000, Ma=0.5, $\alpha = 0°$

We start with one of the most popular tests and choose Re=5000, Ma=0.5, $\alpha = 0°$. We do not include artificial diffusion terms for this test. We evaluate the functionals [17]

$$c_D^p = \frac{2}{\rho_\infty u_\infty^2} \int_S p(\mathbf{n} \cdot \psi_d)\, ds, \qquad c_L^p = \frac{2}{\rho_\infty u_\infty^2} \int_S p(\mathbf{n} \cdot \psi_l)\, ds,$$
$$c_D^v = \frac{2}{\rho_\infty u_\infty^2} \int_S (\tau \mathbf{n}) \cdot \psi_d\, ds, \qquad c_L^v = \frac{2}{\rho_\infty u_\infty^2} \int_S (\tau \mathbf{n}) \cdot \psi_l\, ds,$$

with S denoting the airfoil surface, ρ_∞ the far-field density, τ the viscous stress tensor, and (for $0°$ angle of attack) $\psi_d = \begin{pmatrix} 1 & 0 \end{pmatrix}^T$ and $\psi_l = \begin{pmatrix} 0 & 1 \end{pmatrix}^T$. Note that due to $0°$ angle of attack, $c_L^p = c_L^v = 0$ for the exact solution.

Table 1 reports the results for meshes M1 and M2 using both SIPG and NIPG discretization for the physical diffusion term. The results for SIPG and NIPG are very similar. Table 1 also includes reference values reported by other researchers. Our results for the mesh M2 are in very good agreement with these values, whereas the results for mesh M1 are slightly off. This is consistent with our examination of how many cells one needs to resolve the boundary layer. Based on our results from the Blasius test, we need at least roughly 3 cells in the boundary for piecewise cubic polynomials to resolve the layer. This is satisfied for this test for mesh M2 but not for mesh M1.

6.5.2. Re=1000, Ma=1.2, $\alpha = 0°$

In our final numerical test we combine flow around an airfoil with a shock. We follow Hartmann [16] for the test setup. In this test we compare the performance of our method with and without the artificial diffusion terms $\mathcal{B}_{\mathrm{SD}}^{\mathrm{IP}}$ and $\mathcal{B}_{\mathrm{SC}}^{\mathrm{IP}}$.

Figure 6 shows the Mach contour lines for both versions for mesh M1. Without artificial diffusion terms we observe oscillations in the neighborhood of the shock. These are mostly removed when the $\mathcal{B}_{\mathrm{SD}}^{\mathrm{IP}}$ and $\mathcal{B}_{\mathrm{SC}}^{\mathrm{IP}}$ are employed. Away from the shock, the results are very similar.

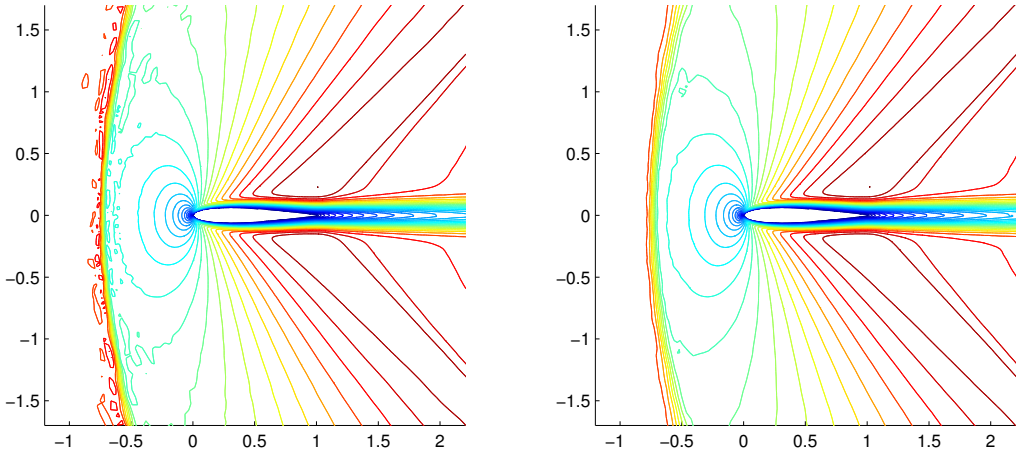

(a) without $\mathcal{B}_{\mathrm{SD}}^{\mathrm{IP}}$ and $\mathcal{B}_{\mathrm{SC}}^{\mathrm{IP}}$

(b) with $\mathcal{B}_{\mathrm{SD}}^{\mathrm{IP}}$ and $\mathcal{B}_{\mathrm{SC}}^{\mathrm{IP}}$

Figure 6: Airfoil test: Results for Mach contours for mesh M1 for Re=1000, Ma=1.2, $\alpha = 0°$.

7. Conclusions

In this paper, we presented two schemes, ST-SDSC-SIPG and ST-SDSC-NIPG, for solving the compressible Navier-Stokes equations. The schemes are based on a spacetime DG approach and use entropy variables as degrees of freedom. The schemes include streamline diffusion and shock-capturing terms that vanish with the correct order of convergence in smooth flow. For the discretization of the physical diffusion terms the NIPG and the SIPG formulation are used, respectively. The resulting schemes satisfy entropy stability estimates. The provided numerical results show that the schemes also perform well numerically. Possible future directions are the extension to three dimensions or to goal-oriented adaptivity, compare, e.g., [18].

Acknowledgments

The authors thank Siddhartha Mishra for many helpful discussions and for providing the resources to make this work possible. S. M. also thanks Miloslav Feistauer for inviting her to a very interesting and stimulating week at the Charles University, Prague. This work was supported by ERC STG. N 306279, SPARCCLE.

A. Proof of entropy stability for inviscid term

Lemma A.1. *Let the assumptions of Theorem 5.3 hold true. And let the input argument* $\mathbf{V}_{K,+}^h$ *in the computation of the numerical inviscid flux at the wall boundary be given by* (35). *Then, there holds*

$$\mathcal{B}_{\mathrm{DG}}(\mathbf{V}^h, \mathbf{V}^h) \geq \int_\Omega S(\mathbf{U}(\mathbf{V}_{N,-}^h(\mathbf{x}))) \, d\mathbf{x} - \int_\Omega S(\mathbf{U}(\mathbf{V}_{0,-}^h(\mathbf{x}))) \, d\mathbf{x}.$$

Proof. The proof of this statement is very similar to the proof of Lemma 2.1, which has been shown as part of Theorem 3.1 in [20]. As that proof is quite long, we do not review the full proof here. Instead we focus on the differences. In [20], $\mathcal{B}_{\mathrm{DG}}$ (using upwind flux in time) is split into temporal terms

$$\begin{aligned}\mathcal{B}^t_{\mathrm{DG}}(\mathbf{V}^h,\mathbf{V}^h) = &-\sum_{n,K}\int_{I^n}\int_K \mathbf{U}(\mathbf{V}^h)\cdot\mathbf{V}^h_t\,d\mathbf{x}\,dt\\ &+\sum_{n,K}\int_K \mathbf{U}(\mathbf{V}^h_{n+1,-})\cdot\mathbf{V}^h_{n+1,-}d\mathbf{x}-\sum_{n,K}\int_K \mathbf{U}(\mathbf{V}^h_{n,-})\cdot\mathbf{V}^h_{n,+}\,d\mathbf{x}\end{aligned}$$

and spatial terms

$$\begin{aligned}\mathcal{B}^s_{\mathrm{DG}}(\mathbf{V}^h,\mathbf{V}^h) = &-\sum_{n,K}\int_{I^n}\int_K\sum_{k=1}^2 \mathbf{F}^k(\mathbf{V}^h)\cdot\mathbf{V}^h_{x_k}\,d\mathbf{x}\,dt\\ &+\sum_{n,K}\sum_{K'\in\mathcal{N}(K)}\int_{I^n}\int_{\partial_{KK'}}\mathbb{F}(\mathbf{V}^h_{K,-},\mathbf{V}^h_{K,+};\nu_{KK'})\cdot\mathbf{V}^h_{K,-}\,d\sigma(\mathbf{x})\,dt.\end{aligned}$$

As $\mathcal{B}^t_{\mathrm{DG}}$ does not include spatial boundary terms, one can follow the proof provided in [20] to show

$$\mathcal{B}^t_{\mathrm{DG}}(\mathbf{V}^h,\mathbf{V}^h)\geq\int_\Omega S(\mathbf{U}(\mathbf{V}^h_{N,-}(\mathbf{x})))\,d\mathbf{x}-\int_\Omega S(\mathbf{U}(\mathbf{V}^h_{0,-}(\mathbf{x})))\,d\mathbf{x}.$$

We are now going to show that

$$\mathcal{B}^s_{\mathrm{DG}}(\mathbf{V}^h,\mathbf{V}^h)\geq 0 \tag{38}$$

still holds true for the case considered in Theorem 5.3. For the considered entropy pair (S,Q), denote by $\psi^k=\mathbf{V}\cdot\mathbf{F}^k-Q^k$, $k=1,2$, the corresponding entropy potential. Then, using $\psi^k_{x_k}=\mathbf{V}_{x_k}\cdot\mathbf{F}^k$ [20, p.115], we get by means of the divergence theorem

$$\begin{aligned}\int_{I^n}\int_K\sum_{k=1}^2\mathbf{F}^k(\mathbf{V}^h)\cdot\mathbf{V}^h_{x_k}\,d\mathbf{x}\,dt &= \int_{I^n}\int_K\sum_{k=1}^2\psi^k(\mathbf{V}^h)_{x_k}\,d\mathbf{x}\,dt\\ &= \sum_{K'\in\mathcal{N}(K)}\int_{I^n}\int_{\partial_{KK'}}\sum_{k=1}^2\psi^k(\mathbf{V}^h_{K,-})\nu^k_{KK'}\,d\sigma(\mathbf{x})\,dt.\end{aligned}$$

This implies

$$\begin{aligned}&\mathcal{B}^s_{\mathrm{DG}}(\mathbf{V}^h,\mathbf{V}^h)=\\ &\sum_{n,K}\sum_{K'\in\mathcal{N}(K)}\int_{I^n}\int_{\partial_{KK'}}\left(-\sum_{k=1}^2\psi^k(\mathbf{V}^h_{K,-})\nu^k_{KK'}+\mathbb{F}(\mathbf{V}^h_{K,-},\mathbf{V}^h_{K,+};\nu_{KK'})\cdot\mathbf{V}^h_{K,-}\right)d\sigma(\mathbf{x})\,dt.\end{aligned} \tag{39}$$

We note that we slightly misused notation in the above considerations by assuming that every cell K has (potentially fictitious) cell neighbors K'. In [20, p.115/116], it is shown under the assumption of compact support inside Ω that (39) implies (38). Here, we show the same claim

for the special case of an edge $e \in \mathcal{F}_{\Gamma_{\text{adia}}}$, which belongs to cell K. Using the definition (8) of the numerical flux, we consider

$$\int_{I^n} \int_e \left(-\sum_{k=1}^{2} \psi^k(\mathbf{V}^h_{K,-}) \nu_e^k + \sum_{k=1}^{2} \left(\mathbb{F}^{k,*}(\mathbf{V}^h_{K,-}, \mathbf{V}^h_{K,+}) \cdot \mathbf{V}^h_{K,-} \right) \nu_e^k \right.$$
$$\left. -\frac{1}{2} \mathbb{D}(\mathbf{V}^h_{K,+} - \mathbf{V}^h_{K,-}) \cdot \mathbf{V}^h_{K,-} \right) d\sigma(\mathbf{x})\, dt. \quad (40)$$

According to (35), we set on e (for given $\mathbf{V}^h_{K,-}$) $\mathbf{V}^h_{K,+} = \left(v^h_{1,K_-}, \quad -v^h_{2,K_-}, \quad -v^h_{3,K_-}, \quad v^h_{4,K_-} \right)^T$. The entropy conservative flux that we use [22] (see [14] for a two-dimensional version) is based on evaluating various arithmetic and logarithmic means. Due to the specific relation of $\mathbf{V}^h_{K,-}$ and $\mathbf{V}^h_{K,+}$, most terms cancel; a short computation shows

$$\mathbb{F}^{1,*}(\mathbf{V}^h_{K,-}, \mathbf{V}^h_{K,+}) = \left(0, \quad p^h_{K_-}, \quad 0, \quad 0 \right)^T \quad \text{and} \quad \mathbb{F}^{2,*}(\mathbf{V}^h_{K,-}, \mathbf{V}^h_{K,+}) = \left(0, \quad 0, \quad p^h_{K_-}, \quad 0 \right)^T.$$

This implies (using (18))

$$\sum_{k=1}^{2} \left(\mathbb{F}^{k,*}(\mathbf{V}^h_{K,-}, \mathbf{V}^h_{K,+}) \cdot \mathbf{V}^h_{K,-} \right) \nu_e^k = p^h_{K_-} v^h_{2,K_-} \nu_e^1 + p^h_{K_-} v^h_{3,K_-} \nu_e^2 = \rho^h_{K_-} u^h_{K_-} \nu_e^1 + \rho^h_{K_-} v^h_{K_-} \nu_e^2.$$

Furthermore, there holds [14, p. 567]

$$\psi^1(\mathbf{V}^h_{K,-}) = \rho^h_{K_-} u^h_{K_-}, \quad \psi^2(\mathbf{V}^h_{K,-}) = \rho^h_{K_-} v^h_{K_-}.$$

Therefore, the terms in the first line of (40) cancel each other. It remains to show that the diffusion operator in the second line results in a non-negative value. We use Rusanov diffusion and consider the following formulation [19]

$$\mathbb{D}(\mathbf{a}, \mathbf{b}; \nu) = \max\left(\lambda_{\max}(\mathbf{U}(\mathbf{a}), \nu), \lambda_{\max}(\mathbf{U}(\mathbf{b}), \nu) \right) \mathbf{U}_{\mathbf{V}} \left(S_{\mathbf{U}} \left(\frac{\mathbf{U}(\mathbf{a}) + \mathbf{U}(\mathbf{b})}{2} \right) \right)$$

with $\lambda_{\max}(\mathbf{U}, \nu)$ denoting the maximum eigenvalue, taken in absolute value, of the Jacobian $\mathbf{F}^1_{\mathbf{U}}(\mathbf{U})\nu^1 + \mathbf{F}^2_{\mathbf{U}}(\mathbf{U})\nu^2$. A short computation shows that the 4×4 matrix $\mathbf{U}_{\mathbf{V}} \left(\widetilde{\mathbf{V}} \right)$ with $\widetilde{\mathbf{V}} = S_{\mathbf{U}} \left(\frac{1}{2} \left(\mathbf{U}(\mathbf{V}^h_{K,-}) + \mathbf{U}(\mathbf{V}^h_{K,+}) \right) \right)$ only has non-zero entries on the diagonal and for indices $(1,4)$ and $(4,1)$. Then, with $p(\widetilde{\mathbf{V}})$ denoting the pressure corresponding to entropy variable $\widetilde{\mathbf{V}}$

$$-\frac{1}{2} \left(\mathbf{V}^h_{K,-} \right)^T \mathbf{U}_{\mathbf{V}} \left(\widetilde{\mathbf{V}} \right) (\mathbf{V}^h_{K,+} - \mathbf{V}^h_{K,-}) = p(\widetilde{\mathbf{V}})(v^h_{2,K_-})^2 + p(\widetilde{\mathbf{V}})(v^h_{3,K_-})^2 \geq 0,$$

which concludes the proof. □

References

[1] D. N. Arnold, F. Brezzi, B. Cockburn, and L. D. Marini. Unified analysis of discontinuous Galerkin methods for elliptic problems. *SIAM J. Numer. Anal.*, 39:1749–1779, 2002.

[2] T. J. Barth. Numerical methods for gasdynamic systems on unstructured meshes. In D. Kröner, M. Ohlberger, and C. Rohde, editors, *An Introduction to Recent Developments in Theory and Numerics of Conservation Laws*, volume 5 of *Lecture Notes in Computational Science and Engineering volume 5*, pages 195–285. Springer, 1999.

[3] T. J. Barth. Space-time error representation and estimation in Navier-Stokes calculations. In S.C. Kassinos, C.A. Langer, G. Iaccarino, and P. Moin, editors, *Complex Effects in Large Eddy Simulations*, volume 56 of *Lecture Notes in Computational Science and Engineering volume 5*, pages 29–48. Springer, 2007.

[4] F. Bassy and S. Rebay. A high-order accurate discontinuous finite element method for the numerical solution of the compressible Navier-Stokes equations. *J. Comput. Phys.*, 131:267–279, 1997.

[5] F. Bassy, S. Rebay, G. Mariotti, S. Pedinotti, and M. Savini. A high-order accurate discontinuous finite element method for inviscid turbomachinery flows. In *Proceedings of the 2nd European Conference on Turbomachinery Fluid Dynamics and Thermodynamics*, pages 99–108, 1997. Antwerp, Belgium.

[6] C. E. Baumann and J. T. Oden. A discontinuous *hp* finite element method for the Euler and Navier-Stokes equations. *Int. J. Numer. Methods Fluids*, 31:79–95, 1999.

[7] S. Brdar, A. Dedner, and R. Klöfkorn. Compact and stable discontinuous Galerkin methods for convection-diffusion problems. *SIAM J. Sci. Comput.*, 34:A263–A282, 2012.

[8] J. Česenek, M. Feistauer, and A. Kosík. DGFEM for the analysis of airfoil vibrations induced by compressible flow. *ZAMM Z. Angew. Math. Mech.*, 93:387–402, 2013.

[9] B. Cockburn and C.-W. Shu. The local discontinuous Galerkin method for time-dependent convection-diffusion systems. *SIAM J. Numer. Anal.*, 35:2440–2463, 1998.

[10] V. Dolejši. On the discontinuous Galerkin method for the numerical solution of the Navier-Stokes equations. *Int. J. Numer. Methods Fluids*, 45:1083–1106, 2004.

[11] V. Dolejši. Semi-implicit interior penalty discontinuous Galerkin methods for viscous compressible flows. *Commun. Comput. Phys.*, 4:231–274, 2008.

[12] V. Dolejší and M. Feistauer. *Discontinuous Galerkin Methods*. Springer, 2015.

[13] M. Feistauer, V. Dolejší, and V. Kučera. On the discontinuous Galerkin method for the simulation of compressible flow with wide range of Mach numbers. *Comput. Visual. Sci.*, 10:17–27, 2007.

[14] U. S. Fjordholm, S. Mishra, and E. Tadmor. Arbitrarily high-order accurate entropy stable essentially nonoscillatory schemes for systems of conservation laws. *SIAM J. Numer. Anal.*, 50:544–573, 2012.

[15] G. Gassner, F. Lörcher, and C.-D. Munz. A discontinuous Galerkin scheme based on a space-time expansion II. Viscous flow equations in multi dimensions. *J. Sci. Comput.*, 34:260–286, 2008.

[16] R. Hartmann. Adaptive discontinuous Galerkin methods with shock-capturing for the compressible Navier-Stokes equations. *Int. J. Numer. Meth. Fluids*, 51:1131–1156, 2006.

[17] R. Hartmann and P. Houston. Symmetric interior penalty DG methods for the compressible Navier-Stokes equations I: Method formulation. *Int. J. Numer. Anal. Model*, 3:1–20, 2006.

[18] R. Hartmann and P. Houston. An optimal order interior penalty discontinuous Galerkin discretization of the compressible Navier-Stokes equations. *J. Comput. Phys.*, 227:9670–9685, 2008.

[19] A. Hiltebrand. *Entropy-stable discontinuous Galerkin finite element methods with streamline diffusion and shock-capturing for hyperbolic systems of conservation laws*. PhD thesis, Seminar for Applied Mathematics, ETH Zurich, 2014.

[20] A. Hiltebrand and S. Mishra. Entropy stable shock capturing space-time discontinuous Galerkin schemes for systems of conservation laws. *Numer. Math.*, 126:103–151, 2014.

[21] T. J. R. Hughes, L. P. Franca, and M. Mallet. A new finite element formulation for computational fluid dynamics: I. Symmetric forms of the compressible Euler and Navier-Stokes equations and the second law of thermodynamics. *Comput. Methods Appl. Mech. Engrg.*, 54:223–234, 1986.

[22] F. Ismail and P. L. Roe. Affordable, entropy-consistent Euler flux functions II: Entropy production at shocks. *J. Comput. Phys.*, 228:5410–5436, 2009.

[23] J. Jaffre, C. Johnson, and A. Szepessy. Convergence of the discontinuous Galerkin finite element method for hyperbolic conservation laws. *Math. Model. Meth. Appl. Sci.*, 5(3):367–386, 1995.

[24] C. Johnson and A. Szepessy. On the convergence of a finite element method for a nonlinear hyperbolic conservation law. *Math. Comp.*, 49(180):427–444, 1987.

[25] C. Johnson, A. Szepessy, and P. Hansbo. On the convergence of shock-capturing streamline diffusion finite element methods for hyperbolic conservation laws. *Math. Comp.*, 54(189):107–129, 1990.

[26] C. M. Klaij, J. J. W. van der Vegt, and H. van der Ven. Pseudo-time stepping methods for space-time discontinuous Galerkin discretizations of the compressible Navier-Stokes equations. *J. Comput. Phys.*, 219:622–643, 2006.

[27] C. M. Klaij, J. J. W. van der Vegt, and H. van der Ven. Space-time discontinuous Galerkin method for the compressible Navier-Stokes equations. *J. Comput. Phys.*, 217:589–611, 2006.

[28] S. May. Spacetime discontinuous Galerkin methods for convection-diffusion equations. In *Bull. Braz. Math. Soc., New Series*, pages 561–573. Sociedade Brasileira de Matematica, 2016.

[29] S. May. Spacetime discontinuous Galerkin methods for solving convection-diffusion systems. *ESAIM Math. Model. Numer. Anal.*, 2017.

[30] P.-O. Persson and J. Peraire. Newton-GMRES preconditioning for discontinuous Galerkin discretizations of the Navier-Stokes equations. *SIAM J. Sci. Comput.*, 30:2709–2733, 2008.

[31] P.-O. Persson and G. Strang. A simple mesh generator in MATLAB. *SIAM Review*, 46:329–345, 2004.

[32] L. Pesch. *Discontinuous Galerkin finite element methods for the Navier-Stokes equations in entropy variable formulation.* PhD thesis, University of Twente, 2007.

[33] Ch. Schwab. *p- and hp-Finite Element Methods.* Oxford University Press, 2004.

[34] F. Shakib, T. J. R. Hughes, and Z. Johan. A new finite element formulation for computational fluid dynamics: X. The compressible Euler and Navier-Stokes equations. *Comput. Methods Appl. Mech. Engrg.*, 89:141–219, 1991.

[35] R. C. Swanson and S. Langer. Comparison of NACA 0012 laminar flow solutions: structured and unstructured grid methods. Technical report, National Aeronautics and Space Administration, Langley Research Center, 2016.

[36] E. Tadmor. The numerical viscosity of entropy stable schemes for systems of conservation laws, I. *Math. Comp.*, 49:91–103, 1987.

[37] E. Tadmor and W. Zhong. Entropy stable approximations of Navier-Stokes equations with no artificial numerical viscosity. *J. Hyperbolic Differ. Equ.*, 3:529–559, 2006.

[38] T. Warburton and J. S. Hesthaven. On the constraints in hp-finite element trace inverse inequalities. *Comput. Methods Appl. Mech. Engrg.*, 192:2765–2773, 2003.

[39] M. Zakerzadeh and G. May. Entropy stable discontinuous Galerkin scheme for the compressible Navier-Stokes equations. In *55th AIAA Aerospace Sciences Meeting*, 2017. Paper AIAA 94-0415.